JOURNAL OF MATERIALS SCIENCE 27 (1992) 2979–2999

Influence of transition metal oxide additions on the crystallization kinetics, microstructures and thermal expansion characteristics of a lithium zinc silicate glass

I. W. DONALD, B. L. METCALFE
Atomic Weapons Establishment, Aldermaston, Reading, Berkshire RG7 4P4, UK
A. E. P. MORRIS
Department of Materials Science, University of Bath, Calverton Down, Bath, UK

Lithium zinc silicate glasses can be used to prepare moderately high thermal expansion glass-ceramics, and these materials are ideally suited for the manufacture of hermetic seals to both nickel-based superalloys and stainless steel. On the basis of earlier work by the present authors, one particular composition from the lithium zinc silicate system was chosen for detailed investigation. This composition contains Na_2O and B_2O_3 fluxing agents, together with P_2O_5 as the primary nucleating agent. The crystallization kinetics and resultant microstructures of this composition have been studied as a function of the heat-treatment parameters using differential thermal analysis, dynamic mechanical thermal analysis, scanning and transmission electron microscopy, ambient and high-temperature X-ray diffraction, and small-angle neutron scattering. Indirect evidence from the dynamic mechanical thermal analysis and small-angle neutron scattering suggests that the nucleated glass is phase separated on a very fine scale, of the order of 16 nm. A number of crystalline phases have been positively identified in the heat-treated glasses, including cristobalite, quartz, tridymite, β_1-Li_2ZnSiO_4 and γ_0-Li_2ZnSiO_4, the precise phases that are formed depending strongly on the heat-treatment parameters. The influence of a number of transition metal oxide additions on the resultant properties of the lithium zinc silicate composition has also been investigated, and it has been shown that the crystallization kinetics, microstructures and thermal expansion characteristics are all strongly affected by these additions. In particular, the activation energy for crystallization (which is related to the nucleating efficiency) is dependent on the ionic field strength of the transition metal ion species employed, with crystallization being favoured by solutes of high field strength.

1. Introduction

Lithium zinc silicate (LZS) glasses containing relatively high concentrations of ZnO can be employed for the preparation of moderately high thermal expansion glass-ceramics. These materials, first reported in 1963 by McMillan and Partridge [1], were subsequently shown to be useful for the manufacture of seals to a variety of metals, including stainless steel [2–9]. More recently, it has been shown that LZS glass-ceramics are also ideal candidates for applications involving sealing to nickel-based superalloys [10, 11]. In addition, it has been re-confirmed that they are indeed ideal materials for bonding to stainless steel [12].

In principle, a number of glass-ceramic systems could be used to give the characteristics required for sealing to moderately high thermal expansion metals and alloys. Materials from the lithium zinc silicate system do, however, offer a number of distinct advantages over other candidates. These include excellent glass-forming ability over a wide composition range, moderate sealing temperatures ($< 1000\,^{\circ}C$) coupled with high fluidity and excellent wetting characteristics, high electrical resistivity, and good chemical durability. Despite these excellent attributes, however, only limited additional work has been reported [10–18] on this versatile glass-ceramic system since the early studies of McMillan and co-workers [1–9].

On the basis of earlier work by the present authors [15], where a number of different LZS compositions were studied, a single composition was chosen for more detailed examination. This recent work has included an assessment of the influence of heat-treatment parameters on the crystallization kinetics and resultant microstructures of this material, together with a comprehensive analysis of the thermal expansion behaviour. In addition, the effect of a number of transition metal oxide, TMO, solutes on the resultant microstructures and properties has been

0022–2461

examined. We report and discuss the results of these investigations. The effect of some of the additives on the sealing characteristics has been reported elsewhere [10–12].

2. Experimental procedures

2.1. Preparation of glass samples

A 200 kg batch of LZS glass was prepared for us by Ceramic Developments (Midlands) Ltd, in the form of granular frit produced by pouring molten glass into demineralized water. The analysed composition of this glass is given in Table I. From this bulk glass, 500 g batches of modified glass were prepared containing the transition metal oxide additions summarized in Table II. These batches were made by mixing the appropriate oxide additives with LZS glass frit and melting at 1450 °C for 1 h in a Pt–5% Rh alloy crucible fitted with a lid. After melting, the glass was poured into demineralized water, dried and re-melted in order to obtain a homogeneous product. As-quenched powder samples for differential thermal analysis (DTA) were prepared by pouring molten glass into demineralized water and sieving the resultant material into standard particle size fractions of 0.6–1.0 mm and $\leqslant 212\ \mu m$. Bar samples of size $\approx 5\ mm \times 5\ mm \times 50\ mm$ together with solid cylinders of diameter 38 mm were prepared by casting glass into graphite moulds pre-heated to 450 °C. These samples were immediately annealed for 1 h, and then furnace cooled at $\approx 0.5\ °C\ min^{-1}$ to room temperature. The annealing temperature for each glass composition employed was based on prior knowledge of the glass transition temperature, T_g, as determined by differential thermal analysis. A small quantity (1 kg) of the equivalent ternary lithium zinc silicate glass was also prepared by melting the constituent batch materials as described above for the doped LZS glasses. The composition of this glass is also given in Table II.

2.2. Conversion of glass to glass-ceramic

The glass cylinders and bars were cut into suitably sized samples using a diamond wheel and then thoroughly cleaned, as described previously [15], in order to remove all surface contaminants which may give rise to preferential surface crystallization during heat treatment. Samples were subsequently heat treated under a variety of conditions, employing a Wentgate Model 0810 vacuum furnace, modified to operate under a positive pressure (35 kPa) of argon. For some of the work, a simulated high-temperature sealing stage was performed in addition to standard nucleation and crystallization heat-treatment cycles, as depicted in Fig. 1.

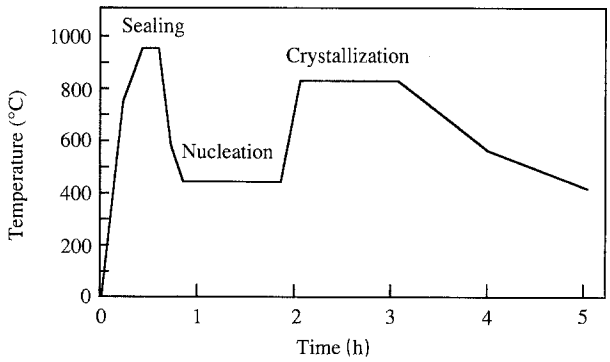

Figure 1 Representative heat-treatment schedule.

TABLE I Composition of the main glass employed in present work (analysed mol %)

Li_2O	Na_2O	ZnO	B_2O_3	P_2O_5	SiO_2
17.84	5.25	17.73	4.31	1.23	53.64

2.3. Measurement of thermal properties

2.3.1. Differential thermal analysis

The thermal properties of the glasses, in the form of as-quenched powder, were monitored using a Stanton Redcroft differential thermal analyser Model 674. The DTA was calibrated over a range of temperatures and heating rates using standard materials (e.g. K_2SO_4 and Ag_2SO_4).

A preliminary assessment of the efficiency of a given nucleating agent or additive was made using the method of Thakur and Thiagarajan [19], in which the variation in peak crystallization temperature with particle size is monitored. Optimum nucleating temperatures were also measured using the method of Marotta *et al.* [20–23]. In the present work, a standard glass particle size of 0.6–1.0 mm was employed, and samples were nucleated *in situ* in the DTA for 1 h in the temperature range 400–620 °C. Peak crystallization temperatures were then monitored by heating the samples through the crystallization range at $10\ °C\ min^{-1}$. Optimum nucleating times were assessed by holding at the optimum nucleating temperature, as determined by the above method, for various periods of time, this procedure again being carried out in the DTA.

TABLE II Compositions of other glasses employed in present work (mol %)

Glass code	Li_2O	Na_2O	ZnO	B_2O_3	P_2O_5	SiO_2	M_xO_y[a]
LZS-M1	17.66	5.20	17.55	4.27	1.22	53.10	1.00
LZS-M2	17.49	5.15	17.37	4.22	1.21	52.56	2.00
LZS-M3.5	17.22	5.06	17.11	4.16	1.19	51.76	3.50
LZS-M5	16.95	4.99	16.84	4.09	1.17	50.96	5.00
Ternary LZS	20.01	–	19.95	–	–	60.01	–

[a] M_xO_y = TiO_2, ZrO_2, HfO_2; V_2O_5, Nb_2O_5, Ta_2O_5; Cr_2O_3, MoO_3, WO_3; NiO, CuO.

Apparent activation energies for crystallization were determined employing the modified Kissinger method, as described by Matusita *et al.* [24–26]. In this non-isothermal, continuous heating rate method, the following relationship is used

$$\ln(\dot{T}^n/T_p^2) = -(mE/RT_p) + \text{constant} \quad (1)$$

where $\dot{T}$ is the heating rate, T_p is the peak crystallization temperature at a given heating rate, E is the apparent activation energy, R is the gas constant, and m and n are numerical factors which are dependent on the crystallization mechanism. The values that n and m can take are summarized in Table III. For the case in which $n = m = 1$, surface crystallization is generally the predominant crystallization mechanism. Equation 1 then reduces to the standard Kissinger equation [27]. On the other hand, it has been proposed [24–26] that the situation corresponding to $n = m = 3$ is obtained for well-nucleated samples in which *bulk* crystallization occurs by the three-dimensional growth of crystals. The activation energy is found from the slope $(-mE/R)$ of a plot of $\ln(\dot{T}^n/T_p^2)$ against $1/T_p$, on substitution of the appropriate values for n, m and R.

For the majority of activation energy determinations, a standard nucleation time of 2 h was employed, this being carried out *in situ* in the DTA using 165 ± 5 mg as-quenched powder of particle size 0.6–1.0 mm. For these samples, values of $n = m = 3$ would be considered most appropriate for substitution into Equation 1. Nominal heating rates of 1–7.5 °C min^{-1} were employed in these studies, with actual rates being determined directly from the temperature chart.

2.3.2. Dynamic mechanical thermal analysis

In addition to standard DTA, the relaxation spectroscopy technique of dynamic mechanical thermal analysis (DMTA) was also employed. In this method, a sinusoidal stress is applied to a clamped sample and the resultant strain is measured as a function of frequency and temperature. Although used widely in the organic polymer field, the technique has only relatively recently been successfully applied to the investigation of higher temperature inorganic glasses (e.g. [28, 29]). In the present work, a Polymer Laboratories Mkll DMTA with an operating temperature up to 800 °C was employed. Samples in the form of bars 1 mm × 5 mm × 10 mm in size were heated at 5 °C min^{-1} in the single-frequency mode at 1 Hz.

TABLE III Determination of activation energies for crystallization (values for numerical parameters n and m; after Matusita *et al.* [24–26])

Crystallization mechanism	n	m
Surface crystallization	1	1
Bulk crystallization with a constant number of nuclei (i.e. a well-nucleated sample)		
three-dimensional growth	3	3
two-dimensional growth	2	2
one-dimensional growth	1	1
Bulk crystallization with an increasing number of nuclei, N (i.e. an as-quenched sample where $N \propto 1/\dot{T}$)		
three-dimensional growth	4	3
two-dimensional growth	3	2
one-dimensional growth	2	1

2.3.3. Thermal expansion characteristics and temperature–viscosity behaviour

The thermal expansion characteristics of the materials in the form of bars measuring approximately 5 mm × 5 mm × 40 mm in size were monitored at a heating rate of 5 °C min^{-1} using a dilatometer supplied by Ceramic Developments (Midlands) Ltd. A minimum of three samples was employed for each determination. The viscosity of the LZS glass was measured as a function of temperature employing standard techniques at both low (≈ 450–500 °C) and high (up to 1550 °C) temperatures.

2.4. X-ray diffraction and small-angle neutron scattering

Both as-cast glass and heat-treated samples were examined using a Philips PW1710 diffractometer employing CuK_α radiation in the range $2\theta = 5$–100°. Some samples were also analysed at Birkbeck College, London, using a Siemens D500 high-temperature X-ray diffractometer employing CuK_α radiation from $2\theta = 10°$–75° in the temperature range ambient to 650 °C. Some nucleated samples of glass were examined by small-angle neutron scattering, SANS, at the Rutherford Laboratory small-angle neutron scattering facility.

2.5. Microstructure

Microstructures were investigated using optical and scanning electron microscopy (SEM) after polishing samples to a 1 μm surface finish. Samples for SEM were coated with Au–Pd alloy prior to examination and were imaged using back-scattered electrons at 20 kV employing a Cambridge S360 scanning electron microscope fitted with an energy dispersive X-ray spectrometer. This technique high-lighted variations in the elemental composition of the phases present, in addition to providing X-ray spectra from which qualitative analyses of specific microstructural features could be made. In addition, transmission electron microscopy (TEM) was employed to examine nucleated glass samples. The samples for TEM were prepared by ion-beam thinning and examined using a Jeol 2000FX microscope operating at 200 kV.

3. Results

3.1. Preparation of glasses

In general, the TMO additions dissolved in the base glass readily at the 2 mol % level. A number of exceptions were noted, however, namely ZrO_2 and HfO_2. The maximum amount of these oxides that could be dissolved in the LZS glass, as verified by

chemical analysis, was ~ 1.6 and ~ 0.8 mol %, respectively. In addition, although 2 mol % Cr_2O_3 could be accommodated in the molten glass, some of this crystallized out on cooling the melt. In general, the resultant glasses were transparent and colourless, although vanadium and nickel additions gave brown glasses, copper gave a blue glass, and chromium produced a dark green opaque material. At the higher concentrations, 3.5 mol % MoO_3 gave a milky opal glass, whilst CuO and NiO gave semi-transparent ultramarine and dark brown glasses, respectively. Only CuO could be fully dissolved at the 5 mol % level.

3.2. Thermal properties of glasses

3.2.1. Differential thermal analysis

The thermal properties of the glasses are summarized in Table IV, and representative DTA traces which

TABLE IV Thermal properties of glasses[a]

Glass code	T_g (°C)	T_{xp_1} (°C)	T_{xp_2} (°C)	T_{ms} (°C)	T_{liq} (°C)
LZS	457 ± 2	660 ± 2	729 ± 3	835 ± 4	937 ± 2
LZS Ternary	489 ± 2	735 ± 3	881 ± 1	951 ± 2	1092 ± 2
LZS-Ti2	463 ± 2	703 ± 3	744 ± 3	845 ± 1	955 ± 3
LZS-Zr2	462 ± 2	688 ± 2	744 ± 1	840 ± 1	945 ± 2
LZS-Hf 2	458 ± 2	677 ± 2	738 ± 3	842 ± 1	946 ± 1
LZS-V2	440 ± 2	606 ± 3	747 ± 2	816 ± 4	899 ± 1
LZS-Nb2	474 ± 2	753 ± 3	776 ± 3	870 ± 2	921 ± 3
LZS-Ta2	478 ± 2	736 ± 1	None	871 ± 2	938 ± 6
LZS-Cr1	460 ± 1	674 ± 2	737 ± 1	835 ± 1	934 ± 1
LZS-Cr2	461 ± 3	664 ± 1	732 ± 1	825 ± 3	930 ± 4
LZS-Mo2	454 ± 1	552	733 ± 1	801 ± 2	905 ± 3
LZS-Mo3.5	457 ± 1	535 ± 1	735 ± 1	803 ± 3	902 ± 2
LZS-W2	462 ± 2	663 ± 2	743 ± 1	842 ± 2	920 ± 1
LZS-W3.5	459 ± 4	633 ± 3	743 ± 4	850 ± 2	906 ± 1
LZS-Ni2	458 ± 1	674 ± 1	728 ± 1	834 ± 4	936 ± 2
LZS-Ni3.5	469 ± 2	702 ± 2	747 ± 1	850 ± 5	938 ± 2
LZS-Ni5	464 ± 2	694 ± 4	740 ± 4	841 ± 4	938 ± 4
LZS-Cu2	452 ± 4	650 ± 2	719 ± 2	823 ± 7	935 ± 1
LZS-Cu5	441 ± 1	631 ± 1	703 ± 2	810 ± 2	929 ± 2

[a] T_g, glass transition temperature (mid point).
T_{xp_1}, temperature corresponding to first crystallization peak.
T_{xp_2}, temperature corresponding to second crystallization peak.
T_{ms}, temperature corresponding to start of melting.
T_{liq}, liquidus temperature (end of melting range).

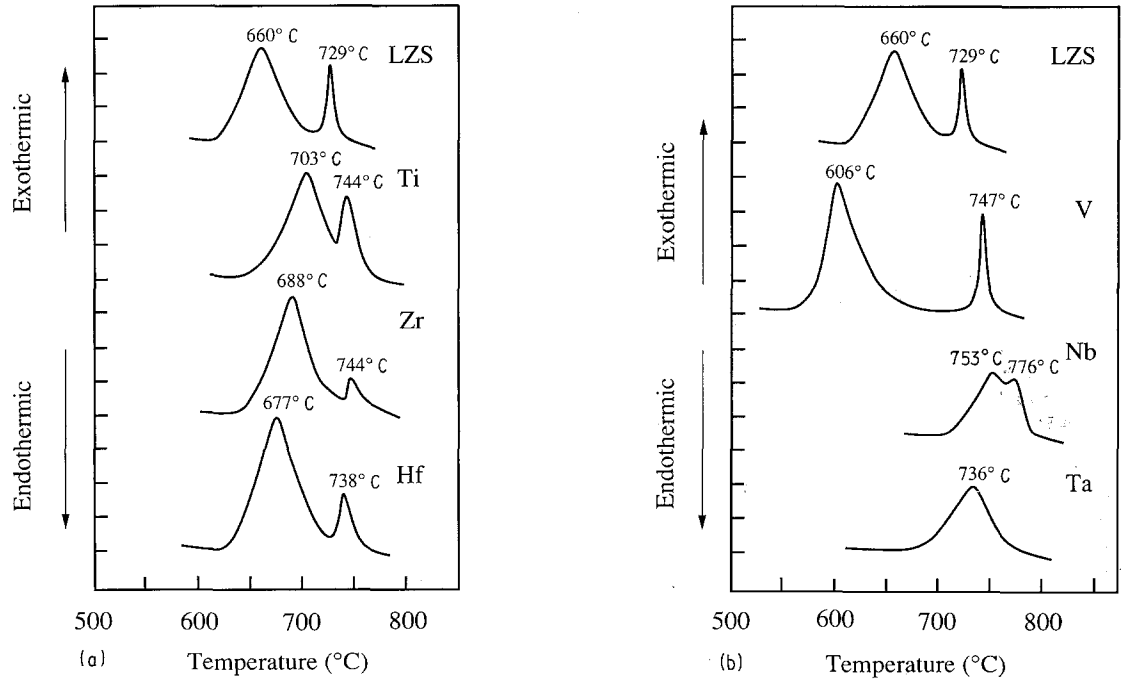

Figure 2 Representative DTA traces for lithium zinc silicate glasses. LZS glass containing (a) 2 mol % Group IV TMO additions; (b) Group V additions; (c) Group VI additions; (d) 3.5 mol % MoO_3 and WO_3.

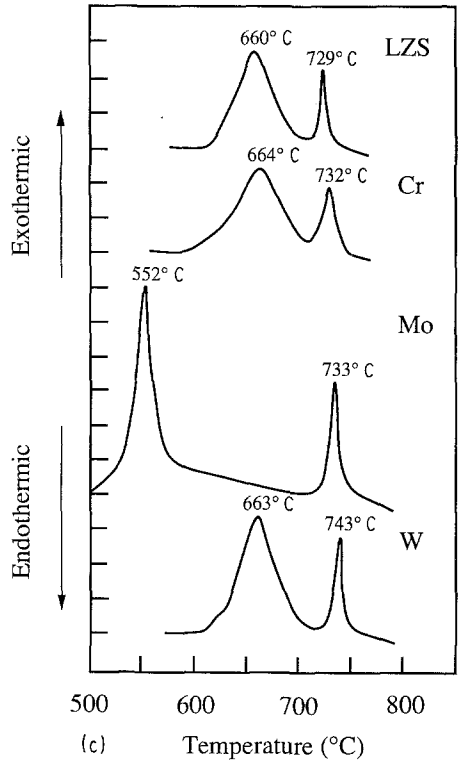

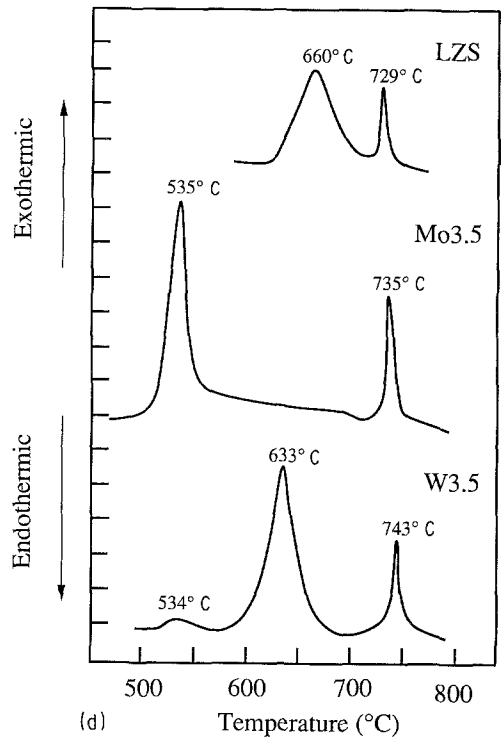

Figure 2 Continued.

illustrate the crystallization behaviour are given in Fig. 2. Two well-resolved crystallization exotherms are apparent for the as-quenched LZS glass, with peaks centred around 660 and 729 °C. The influence of 2 mol % Group IV additions on the crystallization behaviour is shown in Fig. 2a. Group V additions are shown in Fig. 2b and Group VI additions in Fig. 2c. The influence of 3.5 mol % MoO_3 and WO_3 additions is shown in Fig. 2d. Some of the TMO additions have a very pronounced effect on the crystallization behaviour. In particular, molybdenum at the 2 mol % level reduces the temperature of the first crystallization peak from 660 °C to 552 °C, whilst vanadium reduces it to 606 °C. The effect of niobium, on the other hand, is to increase the first crystallization peak to 753 °C, and the two crystallization peaks are partially superimposed. Only a single peak is obtained for tantalum, centred around 736 °C.

Nucleating efficiency data are summarized in Table V. These data suggest that some of the TMO additions improve the overall nucleation efficiency of the as-quenched glass (e.g. Cu, Mo, V and Ni), whilst others decrease it (e.g. Ti, Nb and 3.5% W). Data for determining the optimum nucleating temperature of the LZS glass are given in Fig. 3a, where it may be noted that the main nucleation regime is centred around 465 °C. The effect of time at this optimum temperature is shown in Fig. 3b. Further data are given for 2% Nb and 2% Mo glasses in Fig. 3c and d. The optimum nucleation temperature for the 2% Nb glass is $\approx$ 475 °C. A maximum in ΔT is not apparent for the molybdenum glass due to the proximity of T_g to the first crystallization exotherm. DTA traces illustrating the variation in crystallization behaviour between some as-quenched and nucleated glass samples are shown in Fig. 4. On nucleating the niobium and

TABLE V Effect of small concentrations of transition metal oxide additions on nucleating efficiency of LZS glass

Glass code	Nucleation treatment	ΔT_{xp_1} (°C)	ΔT_{xp_2} (°C)
LZS	None	6	10
LZS	2 h, 465 °C	0	0
LZS Ternary	None	41	13
LZS-Ti2	None	30	4
LZS-Ti2	2 h, 465 °C	3	1
LZS-Zr2	None	8	7
LZS-Hf2	None	1	1
LZS-V2	None	0	14
LZS-Nb2	None	29	25
LZS-Nb2	2 h, 470 °C	6	3
LZS-Ta2	None	7	–
LZS-Cr1	None	8	9
LZS-Cr2	None	6	9
LZS-Mo2	None	0	10
LZS-Mo3.5	None	7	6
LZS-W2	None	6	10
LZS-W3.5	None	28	22
LZS-W3.5	2 h, 465 °C	2	19
LZS-Ni2	None	9	1
LZS-Cu2	None	3	0

tantalum glasses (Fig. 4c), two well-defined crystallization exotherms are resolved. Apparent activation energies for crystallization are summarized in Table VI. Representative activation energy plots are shown in Fig. 5 for the LZS glass. It is clear that the majority of the TMO additions decrease the activation energies for crystallization for both the low and high temperature crystallization peaks. In particular, vanadium, molybdenum and tungsten decrease the activation

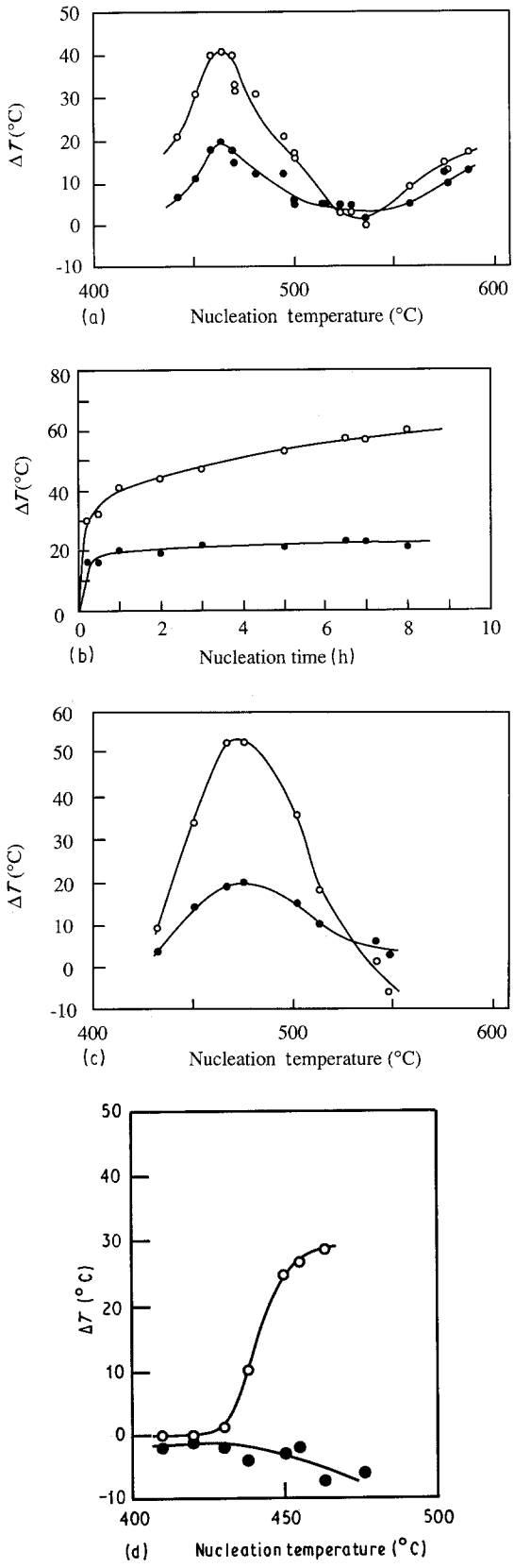

Figure 3 (a) Variation in peak crystallization temperature between as-quenched and nucleated LZS glass ($\Delta T = T_p^o - T_p$) as a function temperature of nucleation. (b) Variation of ΔT with time of nucleation at 465 °C. (c) ΔT as a function of nucleation temperature for the 2% Nb_2O_5 glass. (d) ΔT as a function of nucleation temperature for the 2% MoO_3 glass. (○) First crystallization peak, (●) Second crystallization peak.

energies very markedly. For example, 3.5 mol % Mo decreases the activation energy of the first crystallization peak from 319 to 219 kJ mol^{-1}, and reduces that of the second peak from 389 to 203 kJ mol^{-1}.

TABLE VI Summary of activation energies for crystallization (for values of $n = m = 3$)

Glass code	Nucleation treatment		Activation energy (kJ mol^{-1}): crystallization peak	
	(h)	(°C)	First	Second
LZS	2	465	319	389
LZS	2	585	not resolved	389
LZS-Ti2	2	465	286	329
LZS-Zr2	2	465	294	372
LZS-Hf2	2	465	297	395
LZS-V2	2	465	291	234
LZS-Nb2	2	470	279	303
LZS-Ta2	2	475	279	299
LZS-Cr2	2	465	320	363
LZS-Mo2	2	445	317	220
LZS-Mo3.5	2	445	219	203
LZS-W2	2	465	269	273
LZS-W3.5	2	465	274	183
LZS-Cu2	2	465	341	362
LZS-Cu5	2	460	308	374
LZS-Ni2	2	465	306	342

3.2.2. Dynamic mechanical thermal analysis

DMTA traces for a LZS glass annealed at 400 °C and for a glass nucleated for 1 h at 465 °C are given in Fig. 6. A trace for a nucleated glass that has been subjected to a further crystallization treatment of 1 h at 700 °C is also included in this figure.

3.2.3. Thermal expansion characteristics

The thermal expansion of the annealed and nucleated LZS glass is 11.4×10^{-6} °C^{-1} (20–360 °C). The corresponding value for a glass given a low temperature (400 °C) anneal is 10.5×10^{-6} °C^{-1}. Very characteristic expansion behaviour is found for the glass-ceramics, as illustrated in Fig. 7 for the LZS glass heat treated under different conditions. A region of moderate expansion is noted between ambient and $\approx$ 150 °C. For the majority of the samples a rapid increase in expansion over the range $\approx$ 150–240 °C is then noted, followed by a second region of moderately high expansion up to about 520 °C. Finally, a high-expansion regime is encountered up to the maximum temperature investigated (650 °C). The values of expansion coefficient, α, noted for the glass-ceramics are dependent on the composition as well as the heat-treatment schedule, as summarized in Tables VII and VIII and Figs 8 and 9. Expansion goes through a minimum for T_x within the range $\approx$ 825–900 °C for the LZS glass. The TMO additions modify the expansion behaviour, with titanium, vanadium, molybdenum, tungsten and nickel increasing the expansion coefficient, and zirconium, hafnium and particularly tantalum decreasing α, for a standard heat-treatment schedule.

3.2.4. Temperature–viscosity relationship

The temperature–viscosity behaviour of the LZS is shown in Fig. 10. Direct experimental data could only

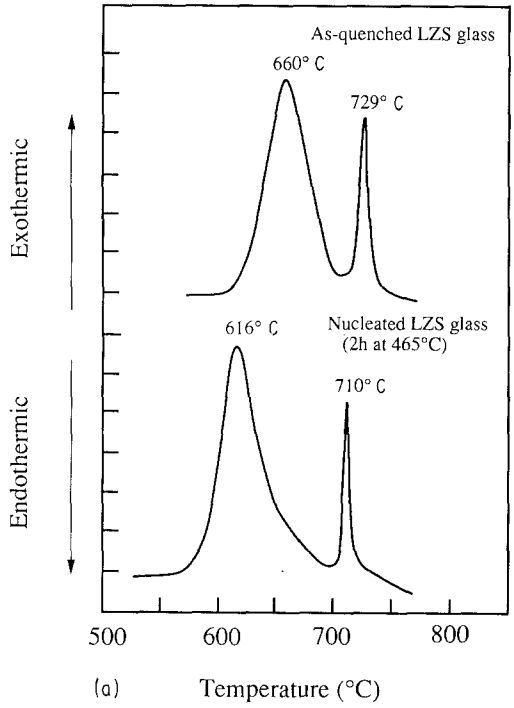

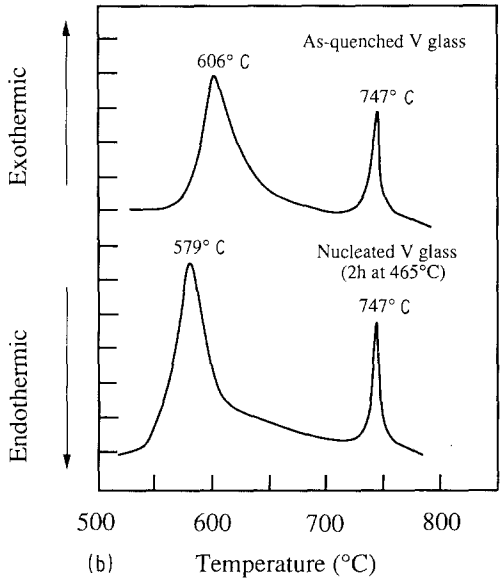

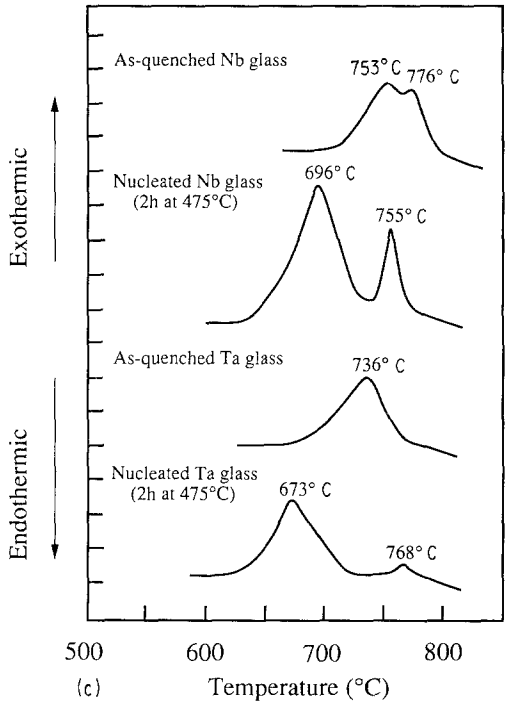

Figure 4 DTA traces comparing as-quenched and nucleated glass samples. (a) LZS glass; (b) LZS glass with 2 mol % V_2O_5; (c) LZS glasses with 2 mol % Nb_2O_5 and Ta_2O_5.

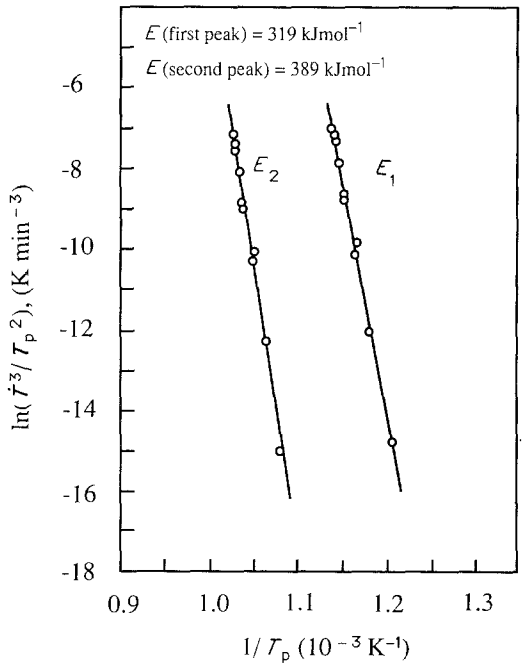

Figure 5 Representative activation energy plots for LZS glass.

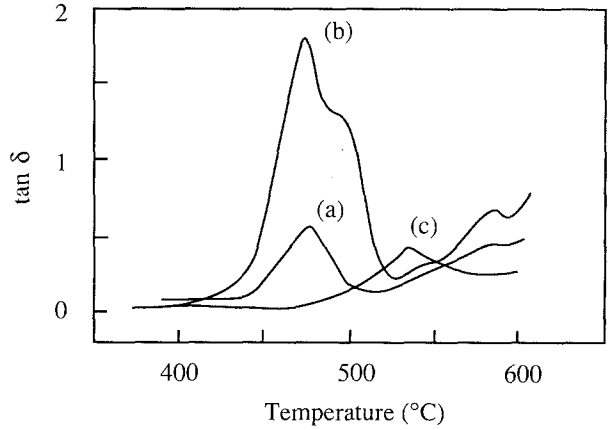

Figure 6 DMTA single frequency plots for (a) an annealed glass, (b) an annealed and nucleated glass, and (c) a glass nucleated and then crystallized for 1 h at 700 °C.

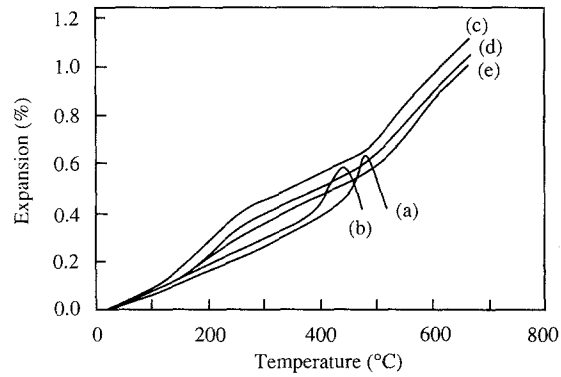

Figure 7 Representative thermal expansion behaviour of LZS glass and glass-ceramics: (a) LZS1, (b) LZS2, (c) LZS11, (d) LZS13, (e) LZS6 (see Table VII for heat-treatment schedules).

TABLE VII Summary of thermal expansion data for LZS glass-ceramics as a function of heat-treatment parameters

Glass code	Heat-treatment schedule						Thermal expansion coefficient ($10^{-6}\,°C^{-1}$)	
	Stage 1		Stage 2		Stage 3		20–460 °C	20–550 °C
	Temperature (°C)	Time (min)	Temperature (°C)	Time (min)	Temperature (°C)	Time (min)		
LZS1 (low temperature anneal)			–	–	–	–	10.5 (20–360)	–
LZS2 (annealed and nucleated)			–	–	–	–	11.4 (20–360)	–
LZS5	–	–	465	60	750	60	14.4	15.7
LZS6	–	–	465	60	800	60	13.0	14.4
LZS7	–	–	465	60	850	60	13.0	14.8
LZS8	–	–	465	60	900	60	14.7	16.0
LZS9	–	–	465	60	950	60	14.0	15.7
LZS11	950	5	465	60	750	60	15.2	16.7
LZS12	950	5	465	60	800	60	15.1	16.4
LZS13	950	5	465	60	850	60	13.9	15.6
LZS14	950	5	465	60	900	60	14.7	16.1
LZS15	950	5	465	60	950	60	14.9	16.1
LZS16	950	5	585	60	850	60	14.3	15.5

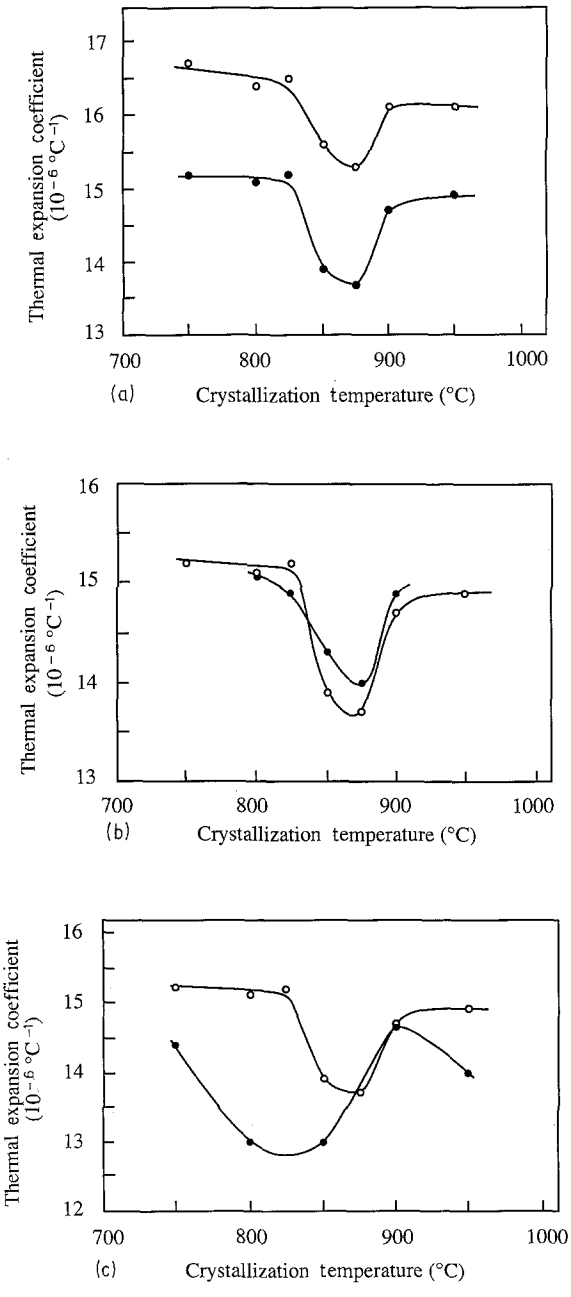

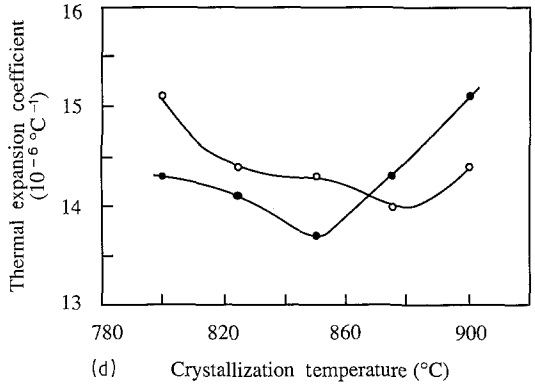

Figure 8 Variation in thermal expansion coefficient of LZS glass-ceramics (quoted values are normally to within $\pm 0.2 \times 10^{-6}\,°C^{-1}$). (a) Standard LZS glass-ceramic (LZS13) over the temperature ranges (●) 20–460 °C and (○) 20–550 °C. (b) LZS glass-ceramics nucleated at (○) low (465 °C) and (●) high (585 °C) temperatures. (c) as a function of the crystallization temperature, (○) with and (●) without high-temperature simulated sealing cycles. (d) LZS glass-ceramics with 2 mol % (○) NiO and (●) CuO.

TABLE VIII Summary of thermal expansion data for LZS glass-ceramics containing transition metal oxide additions (for standard heat treatment of 950 °C/5 min + 465 °C/60 min + 850 °C/60 min)

Glass code	Thermal expansion coefficient ($10^{-6}\,°C^{-1}$)	
	20–460 °C	20–550 °C
LZS	13.9	15.6
LZS-Ti2	14.5	16.2
LZS-Zr2	13.1	13.7
LZS-Hf2	12.9	13.7
LZS-V2	15.8	19.3
LZS-Nb2	13.6	15.0
LZS-Ta2	10.9	11.5
LZS-Cr2	13.4	15.3
LZS-Mo2	14.4	17.3
LZS-W2	14.0	18.4
LZS-Ni2	14.2	15.9
LZS-Cu2	13.7	16.0

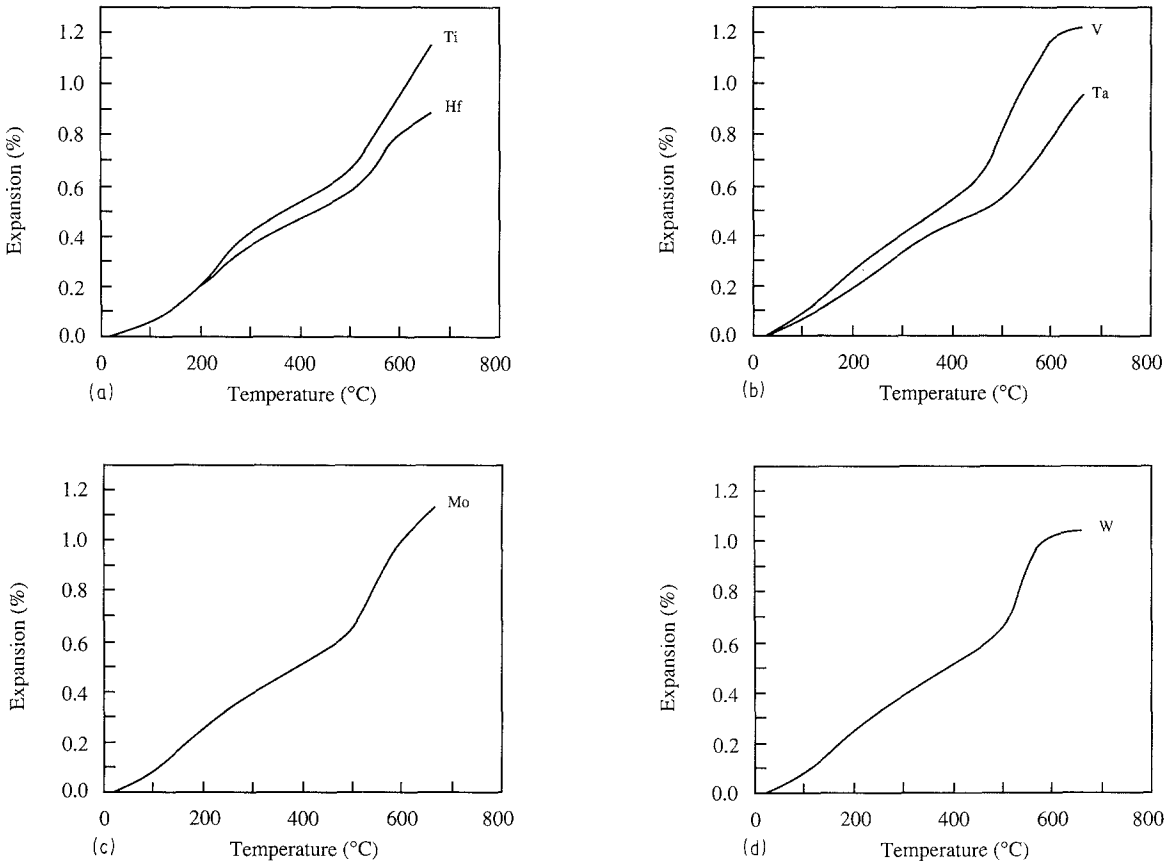

Figure 9 Thermal expansion behaviour of LZS glass-ceramics containing a number of TMO additions: (a) TiO_2 and HfO_2, (b) V_2O_5 and Ta_2O_5, (c) MoO_3, (d) WO_3, (e) CuO.

be obtained over the temperature regimes 430–450 °C and 1000–1400 °C due to changes occurring in the glass as a function of time. Data were derived for the intermediate temperature regime by Fulcher analysis using the relationship

$$\log(\text{viscosity}) = A + B/(T - T_0) \quad (2)$$

where $A = -1.28654$, $B = 2387.9$, and $T_0 = 272.0$, for this particular glass composition.

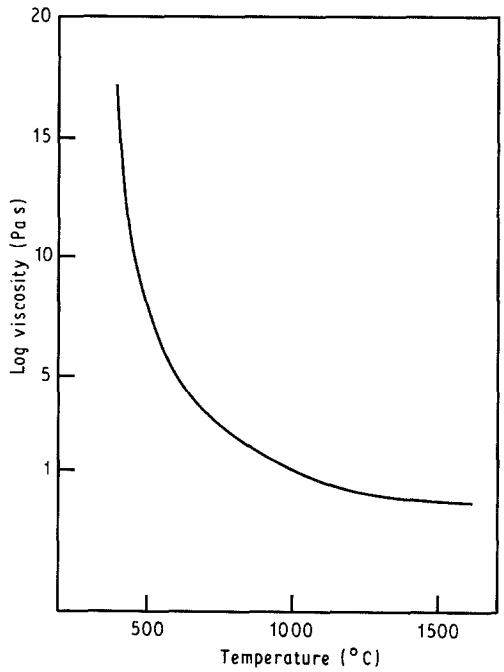

Figure 10 Temperature–viscosity behaviour for LZS glass.

3.3. Crystalline phases present

3.3.1. Ambient temperature X-ray data

Some typical X-ray diffraction data are shown in Fig. 11. The majority of as-cast glasses were fully X-ray amorphous, as were glasses which had undergone nucleation for 1 h at 465 °C. A number of exceptions were noted, however. Both annealed and nucleated glasses containing 2 mol % Cr_2O_3 contained a proportion of $ZnCr_2O_4$ crystals (Fig. 11a). Similar glasses containing 3.5 mol % MoO_3 contained crystals which were most closely related to the β_1-Li_2ZnSiO_4 phase (Fig. 11b). LZS glass nucleated at the higher temperature of 585 °C was partially crystalline and also contained crystals similar to β_1-Li_2ZnSiO_4 (Fig. 11c). Further heat treatment of

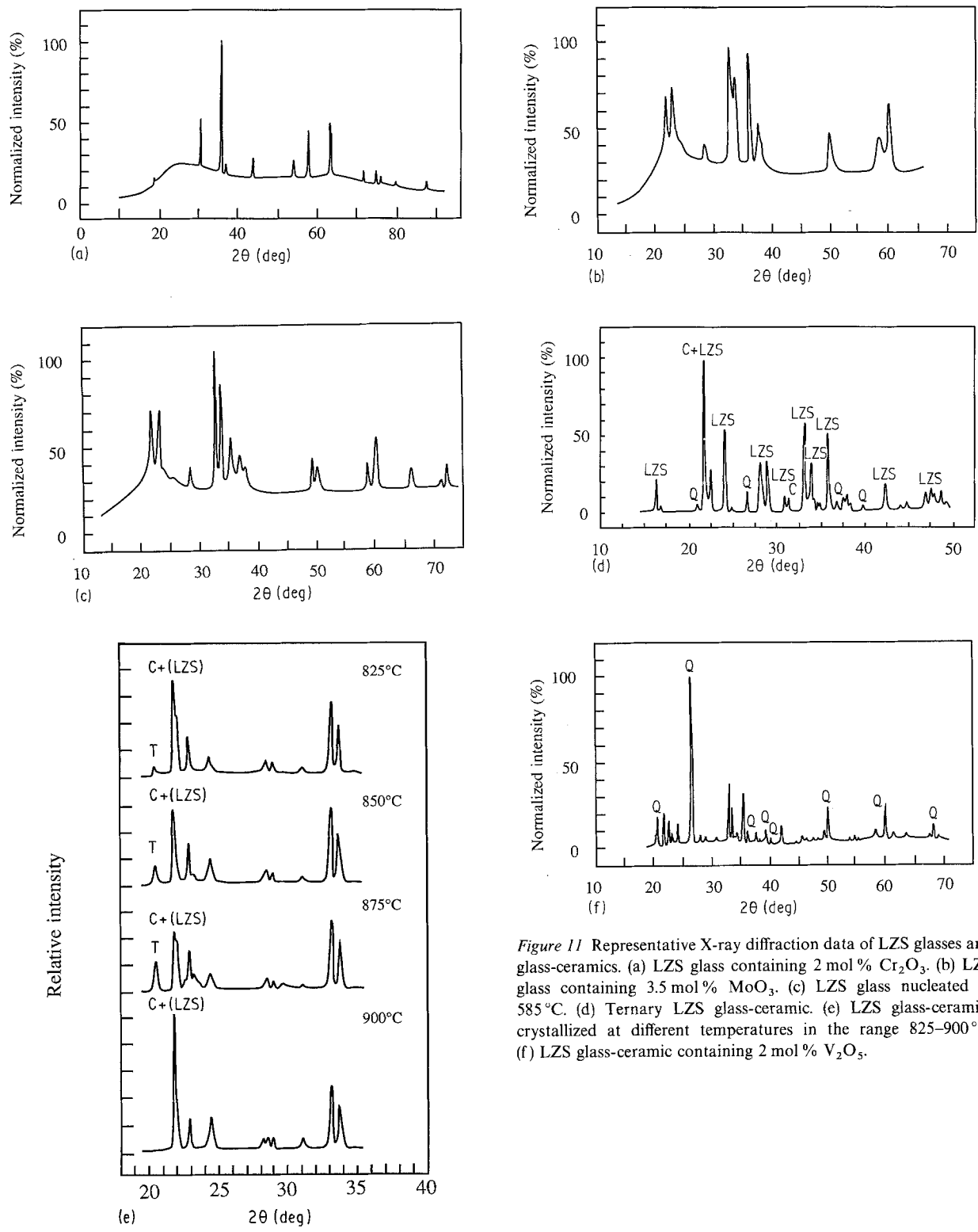

Figure 11 Representative X-ray diffraction data of LZS glasses and glass-ceramics. (a) LZS glass containing 2 mol % Cr_2O_3. (b) LZS glass containing 3.5 mol % MoO_3. (c) LZS glass nucleated at 585 °C. (d) Ternary LZS glass-ceramic. (e) LZS glass-ceramics crystallized at different temperatures in the range 825–900 °C. (f) LZS glass-ceramic containing 2 mol % V_2O_5.

nucleated glasses at temperatures $\geqslant 650\,^{\circ}C$ produced characteristic X-ray peaks which increased in intensity with increasing temperature and time. A number of crystalline phases were identified in these materials including cristobalite, quartz and tridymite, together with phases most closely related to β_1- and γ_0-Li_2ZnSiO_4, as summarized in Table IX. A number of unidentified phases were also present in some of the samples.

3.3.2. High-temperature X-ray data

High-temperature X-ray diffraction data were obtained at a number of different temperatures using a sample of the simple ternary LZS glass-ceramic. The ternary was employed in order to aid in the identification of the phases present. Representative X-ray diffraction data for this glass-ceramic at ambient temperature are given in Fig. 11d, whilst the high-temperature data are summarized in Table IX.

3.3.3. Small-angle neutron scattering data

Data obtained from the small-angle neutron scattering experiment exhibited a strong peak in intensity at low $Q(39 \times 10^{-4}$ nm). This suggests that the

TABLE IX Summary of X-ray diffraction data

Glass Code	Heat-treatment schedule						Crystal phases
	Stage 1		Stage 2		Stage 3		
	Temperature (°C)	Time (min)	Temperature (°C)	Time (min)	Temperature (°C)	Time (min)	
Ambient temperature							
LZS2	–	–	465	60	–	–	Amorphous
LZS3	–	–	585	60	–	–	Amorphous + β_1-Li_2ZnSiO_4
LZS4	–	–	465	60	700	60	Cristobalite + LZS[a]
LZS7	–	–	465	60	850	60	Cristobalite + tridymite + β_1-Li_2ZnSiO_4 + γ_0-Li_2ZnSiO_4
LZS13	950	60	465	60	850	60	Cristobalite + quartz + tridymite + β_1-Li_2ZnSiO_4 + γ_0-Li_2ZnSiO_4
LZS10	–	–	585	60	850	60	Cristobalite + quartz + LZS
LZS16	950	5	585	60	850	60	Cristobalite + quartz + tridymite + LZS
LZS-Cr2	–	–	465	60	–	–	Amorphous + $ZnCr_2O_4$
LZS-Mo3.5	–	–	465	60	–	–	Amorphous + β_1-Li_2ZnSiO_4
LZS-V2	950	5	465	60	850	60	Quartz + LZS
LZS-Cr2	950	5	465	60	850	60	Tridymite + $ZnCr_2O_4$ + LZS
LZS-Mo2	950	5	465	60	850	60	Tridymite + LZS + unidentified phase
High temperature							
Ternary LZS (at ambient temperature)	–	–	465	60	850	60	α-cristobalite + α-quartz + γ_0-Li_2ZnSiO_4
Ternary LZS (at 350 °C)	–	–	465	60	850	60	β-cristobalite + α-quartz + γ_0-Li_2ZnSiO_4
Ternary LZS (at 600 °C)	–	–	465	60	850	60	β-cristobalite + β-quartz + γ_0-Li_2ZnSiO_4 + β_{11}-Li_2ZnSiO_4

[a] LZS, unidentified lithium zinc silicate phase.

glass nucleated for 1 h at 465 °C is phase separated on a very fine scale, of the order of 16 nm.

3.4. Microstructures

3.4.1. Materials not subjected to a high-temperature simulated sealing stage

Optical examination of the LZS glass-ceramic showed the microstructure to consist of fine crystalline grains with some larger acicular grains, but the low reflectivity of the samples prevented a more detailed examination at higher magnifications. Examination by SEM using back-scattered electrons, on the other hand, provided useful data on the microstructures with excellent contrast between the individual phases. Microstructures of the LZS glass-ceramics crystallized at different temperatures are given in Fig. 12. In addition, micrographs of a number of the glass-ceramics containing TMO additions are shown in Figs 13 and 14. For crystallization temperatures $\leqslant 850$ °C the LZS glass-ceramic consists of small equi-axed grains of the order of 0.5–1 μm in size together with larger acicular grains up to ≈ 8 μm in length and residual glass. Data from EDAX analysis suggest that the smaller, lighter coloured grains are the main Li_2ZnSiO_4 phase, whilst the larger acicular grains are silica. The grain size increases when the crystallization temperature is increased from 850 to 900 °C.

It is clear from Figs 13 and 14 that some of the TMO additives have a very pronounced influence on the microstructures obtained. Addition of the Group IV oxides leads to microstructures similar in general appearance to the base glass-ceramic, although titanium apparently gives a coarser microstructure with ≈ 2 μm size equi-axed grains and silica laths up to 12 μm in length. In addition, when viewed at higher magnification, the equi-axed grains appear to consist of groups of small crystal aggregates. Similarly, zirconium and hafnium additions lead to the formation of aggregate crystal clusters. Group V additions give widely differing microstructures. The vanadium microstructure is similar to the base LZS glass-ceramic, but niobium and particularly tantalum are quite different. Longer and thinner silica laths are apparent in the niobium glass-ceramic, and the LZS phase is less equi-axed and more star shaped. With tantalum, on the other hand, the acicular silica phase has been replaced by clusters of equi-axed grains; in addition, a dispersion of small bright crystals rich in tantalum is noted. For Group VI additions, chromium gives an overall microstructure similar to that of the base glass-ceramic; however, dispersed within this are relatively large (up to 6 μm) cubic crystals of zinc chromate, $ZnCr_2O_4$, present as clusters consisting of several individual grains. Addition of molybdenum decreases the grain size of the equi-axed grains markedly to $\leqslant 0.5$ μm, and these crystals are present as discrete individual grains rather than small agglomerates. The grain size is increased for

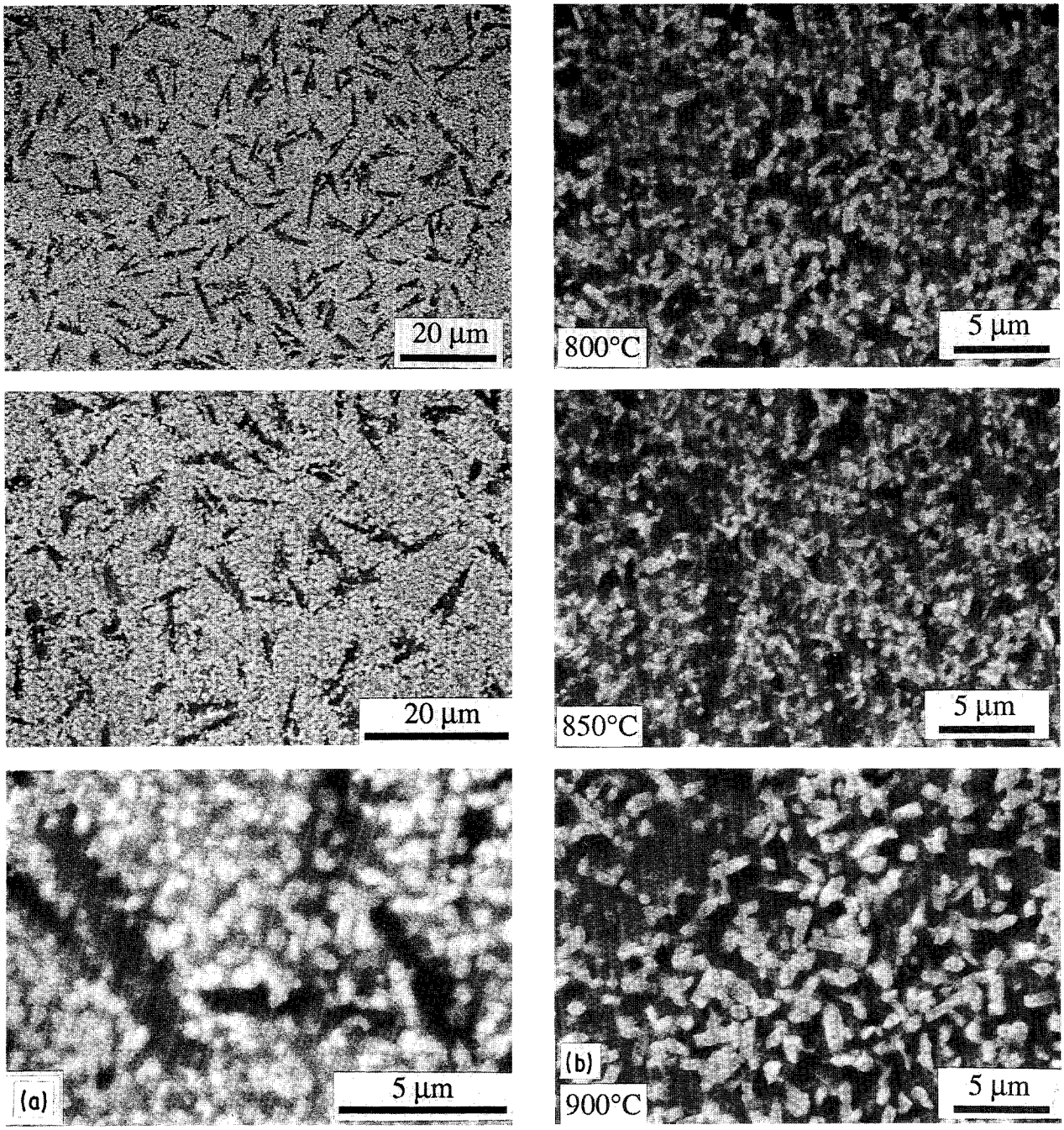

Figure 12 Microstructures of LZS glass-ceramics: (a) LZS7-standard heat-treatment (nucleation and crystallization only; a high-temperature simulated sealing stage has not been included); (b) with inclusion of high-temperature sealing stage, crystallized at different temperatures.

tungsten additions and a dispersion of light and dark spherical particles is also evident, with the light particles being rich in tungsten and silicon. The microstructures of the materials containing NiO and CuO are similar to that of the LZS glass-ceramic, with the NiO giving a slightly coarser grain size.

Some transmission electron micrographs of nucleated samples are shown in Fig. 15. No contrast is seen initially in samples nucleated at 465 °C, although contrast is developed within 1–2 min due to damage induced by the electron beam. Samples nucleated at 585 °C contain spherulitic crystals.

3.4.2. Materials subjected to a high-temperature simulated sealing stage

Glasses which have been subjected to a high-temperature (950 °C) simulated sealing treatment prior to normal nucleation and crystallization exhibit microstructures which are in general remarkably similar to those obtained without the high-temperature stage. Differences are apparent in some cases, however (Figs 16–18). For example, titanium gives a coarser microstructure if a sealing stage is included. In addition, a number of the glass-ceramics which have been subjected to the sealing stage exhibit areas containing dendritic structures. In particular, the chromium glass-ceramics exhibit extensive and very well defined dendritic features. Less extensive structures are also observed with the titanium, nickel and copper materials. The nickel and copper glass-ceramics are of particular interest because when heat-treated in a nominally inert atmosphere, a layer of metallic nickel

or copper is formed on the surface, as illustrated in Fig. 19. These materials also show acicular silica nucleated from the Li_2ZnSiO_4 phase.

4. Discussion

The optimum nucleation temperature for the LZS glass, derived from the DTA data in Fig. 3, is $\approx 465\,^{\circ}C$; this temperature corresponds to the maximum in the ΔT versus $T_{nuc.}$ curve. It is evident from Fig. 3, however, that a second nucleation regime occurs at higher temperatures, although a specific maximum is not observed. Two different nucleation mechanisms are operative, according to the temperature regime employed. In the higher temperature regime, nucleation is due to the formation of $\approx 1\,\mu m$ size crystallites, which are most closely related to β_1-Li_2ZnSiO_4, as noted previously for a similar glass [15], and confirmed for this glass composition by X-ray diffraction (Fig. 11c). Investigation by TEM reveals that these crystallites are spherulitic in nature, as shown in Fig. 15. TEM EDAX spot analyses suggest that the crystallites form by migration of zinc from the glass phase. The mechanism responsible for the major lower temperature nucleation regime is open to greater speculation. When nucleated in this temperature regime glasses are still fully X-ray

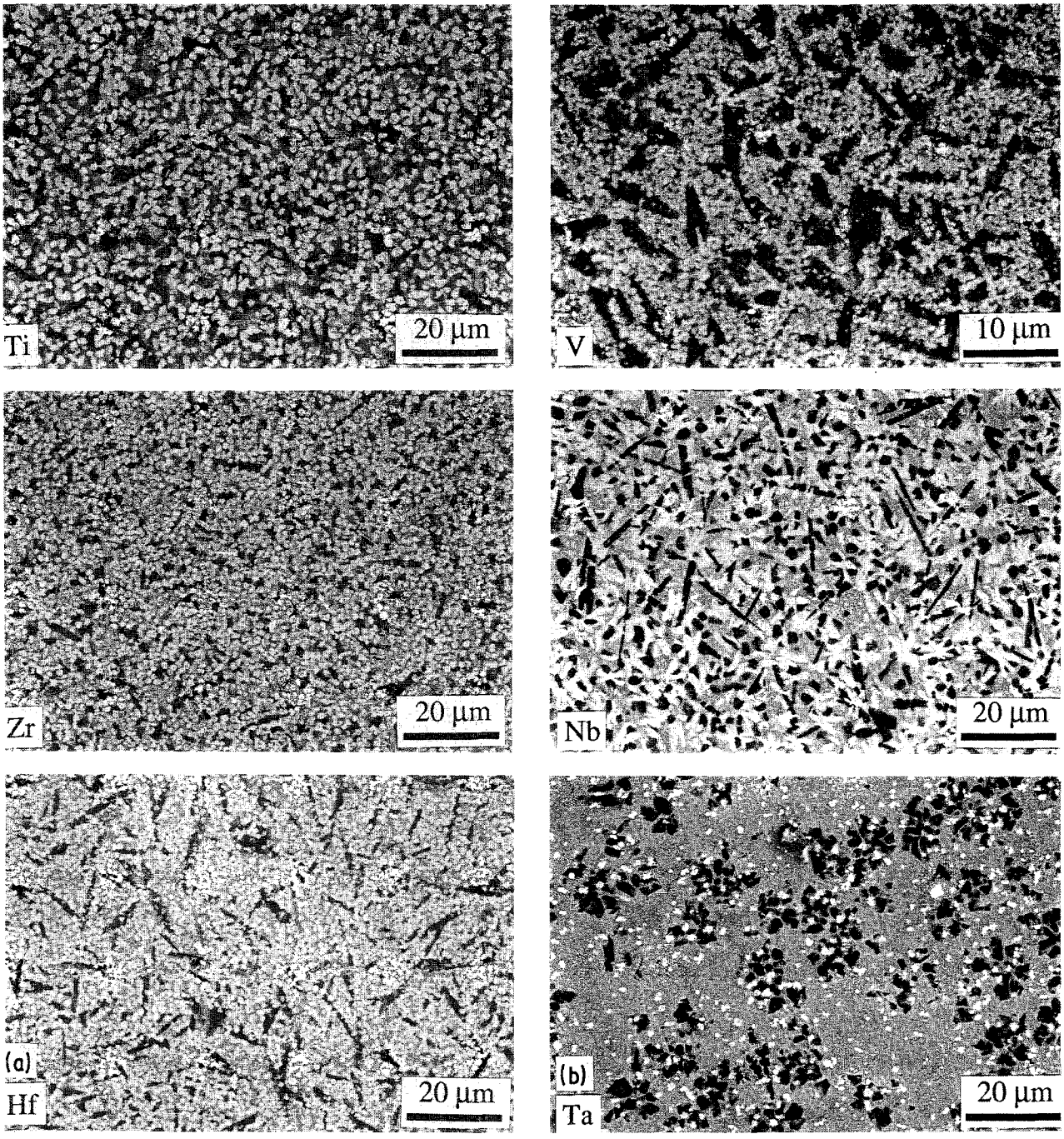

Figure 13 Representative microstructures of LZS glass-ceramics containing TMO additions (with nucleation and crystallization stages only): (a) with Group IV TMO additions; (b) with Group V TMO additions; (c) with Group VI TMO additions.

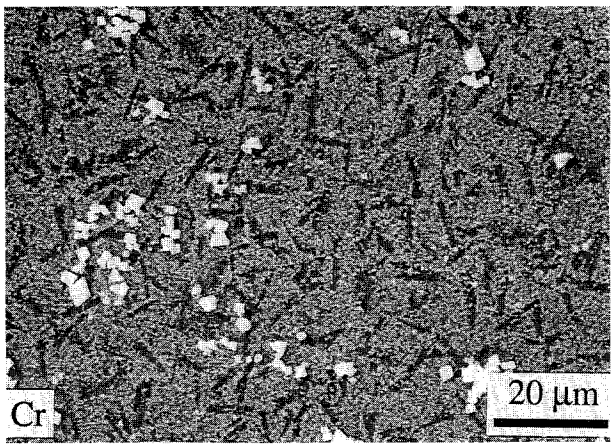

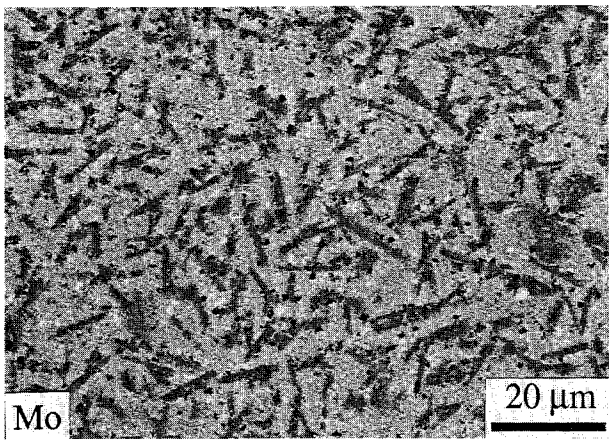

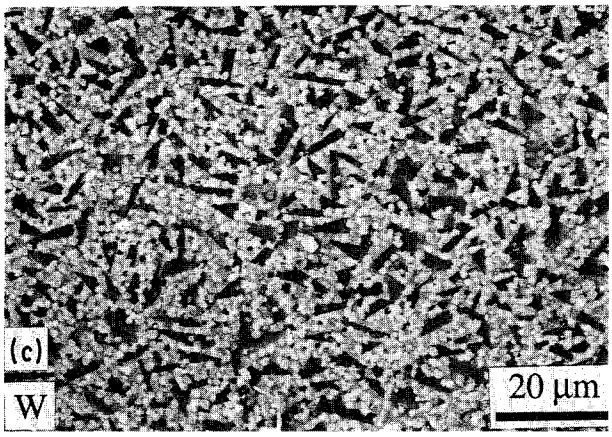

Figure 13 Continued.

amorphous. There is evidence from both DMTA and SANS, however, that the glass has undergone very fine scale amorphous-in-amorphous phase separation. The DMTA data confirm that the nucleated glass exhibits two T_gs, as indicated by the high-temperature shoulder apparent for the nucleated glass in the loss tangent versus temperature plot shown in Fig. 6. In addition, the SANS data suggest that the glass is phase separated on a very fine scale, of the order of 16 nm. Although direct evidence for phase separation from TEM studies is lacking, further indirect evidence for a structural or physical change is available from microhardness measurements. For example, microhardness has been noted to go through a maximum, increasing from $\approx$ 580 VPN for the as-quenched glass to 650 VPN for glass heated for 1 h at 465 °C [30]. It is

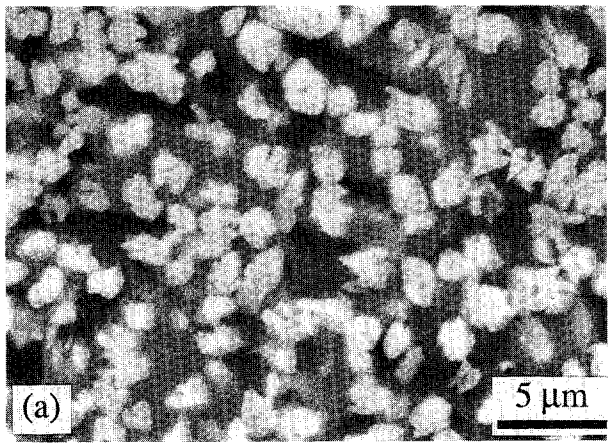

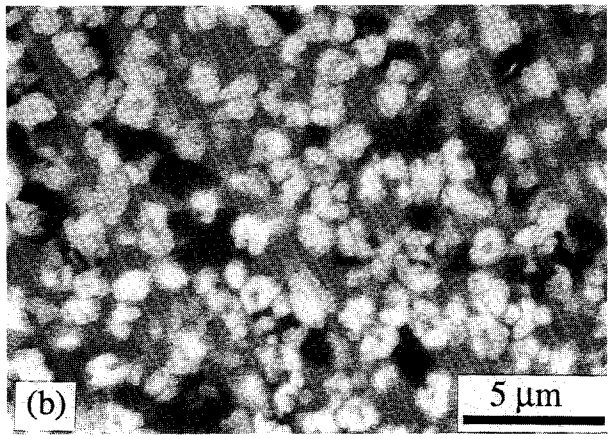

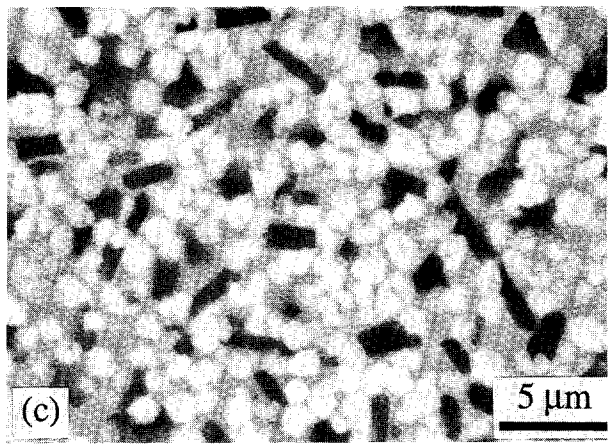

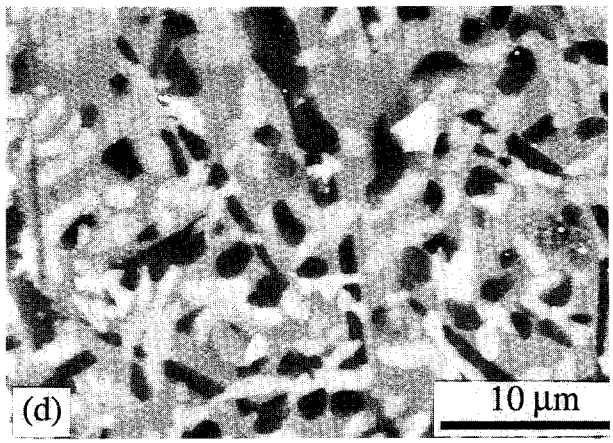

Figure 14 High-magnification micrographs of LZS glass-ceramics containing TMO additions (nucleation and crystallization stages only) with (a) TiO_2, (b) ZrO_2, (c) HfO_2, (d) Nb_2O_5, (e) Ta_2O_5, (f) WO_3.

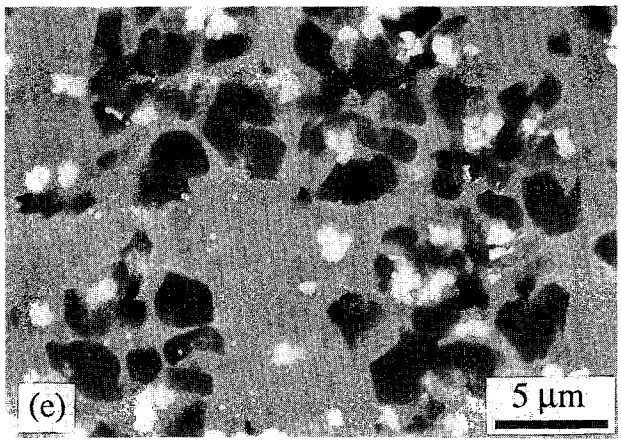

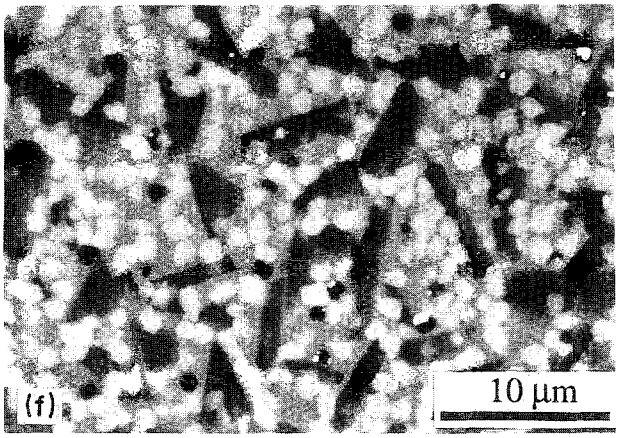

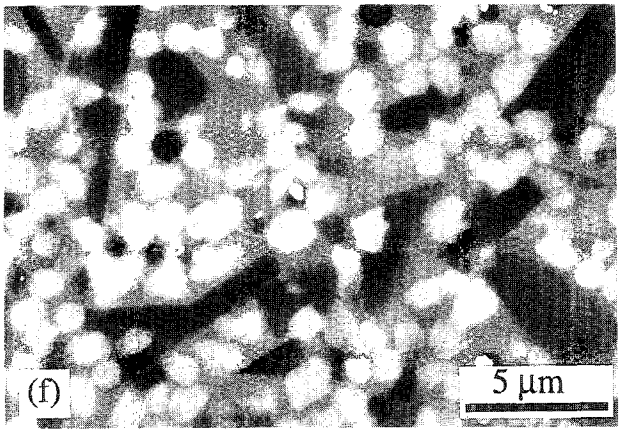

Figure 14 Continued.

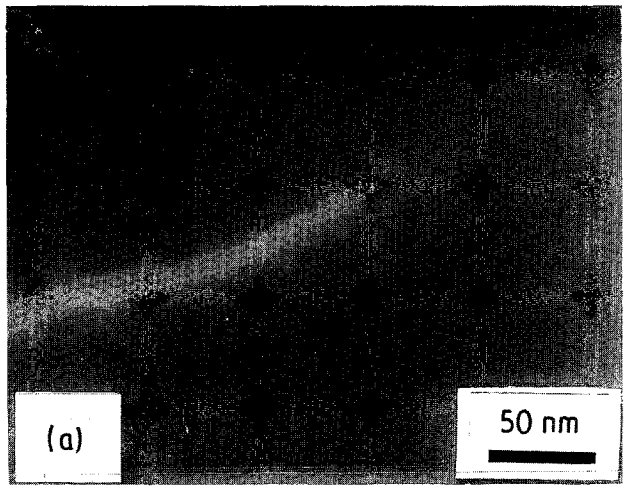

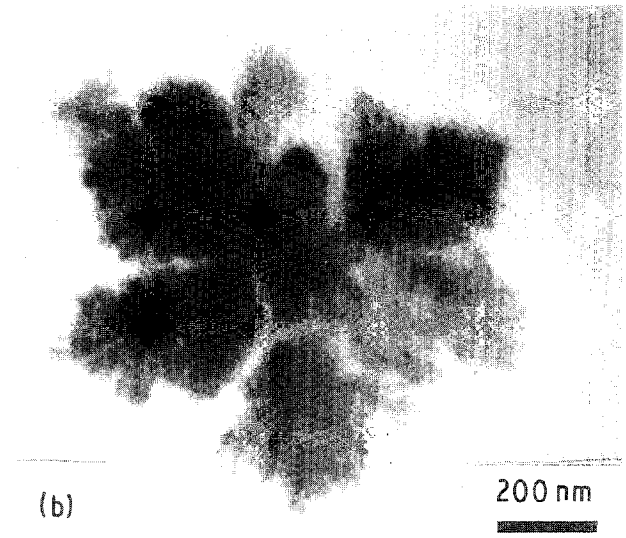

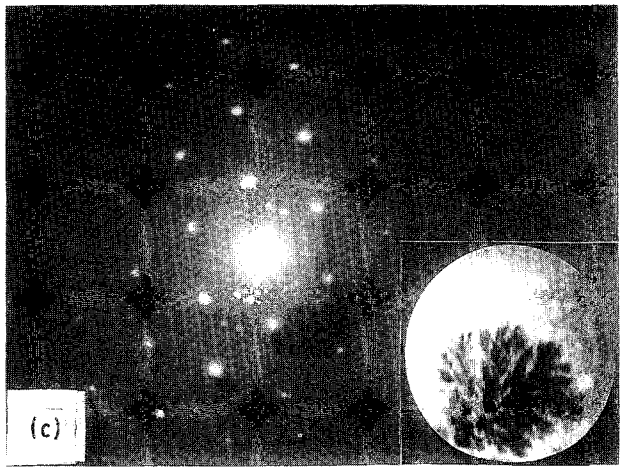

Figure 15 Transmission electron micrographs of nucleated LZS glass samples: nucleated at (a) 465 °C, (b) 585 °C.

likely that phase separation occurs by spinodal decomposition to give a micro-phase separated structure exhibiting little electron contrast between the individual phases.

The ambient and high-temperature X-ray diffraction data indicate that the LZS glass-ceramic contains varying proportions of cristobalite, quartz and tridymite, together with phases most closely related to β_1-Li_2ZnSiO_4 and γ_0-Li_2ZnSiO_4. The precise phases that are formed depend strongly on the heat-treatment parameters employed. The Li_2ZnSiO_4 phases may be present as a solid solution, although individual phases may be present in some instances. The X-ray spectra are very difficult to interpret precisely because the peak positions and corresponding *d*-spacings of the major phase(s) cannot be identified positively with any of the known lithium zinc silicate phases [13, 14, 31], although this may not be surprising due to the influence of the extra additions of Na_2O, B_2O_3 and P_2O_5 to the LZS glass. The data for the "simple" ternary LZS glass-ceramic were, however, more easily and more positively identified (Table IX).

It has been shown that the thermal expansion of the LZS glass-ceramic can be varied over a reasonably

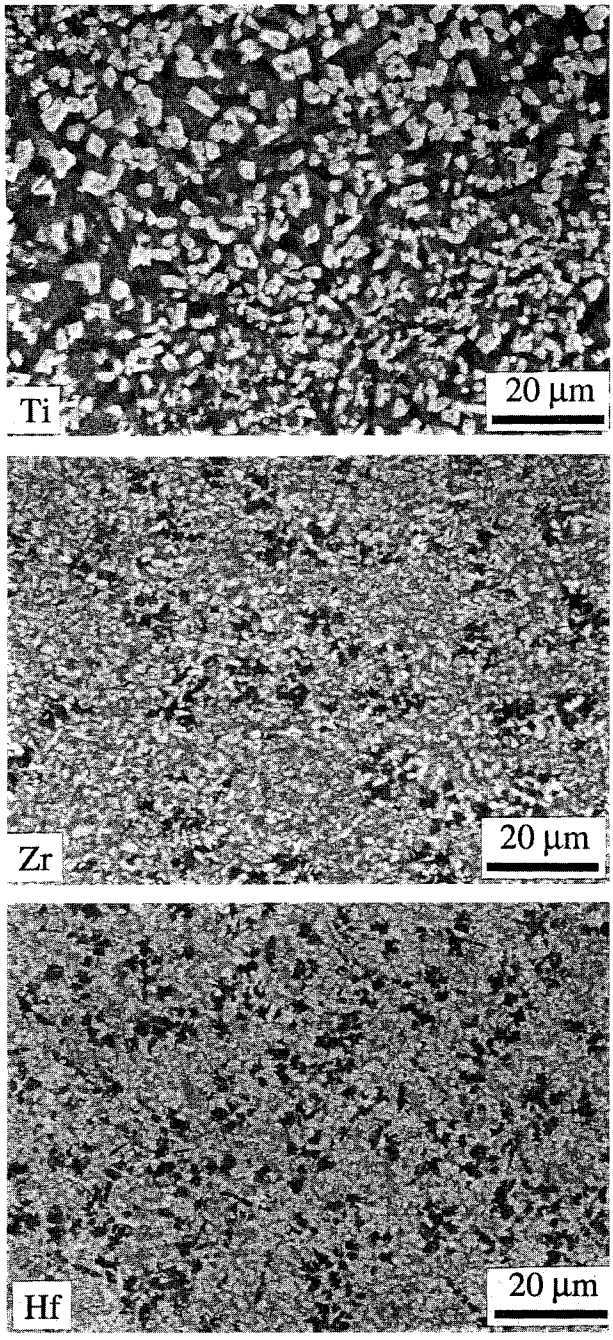

Figure 16 Microstructures of LZS glass-ceramics containing Group IV TMO additions (a high-temperature simulated sealing heat treatment has been included).

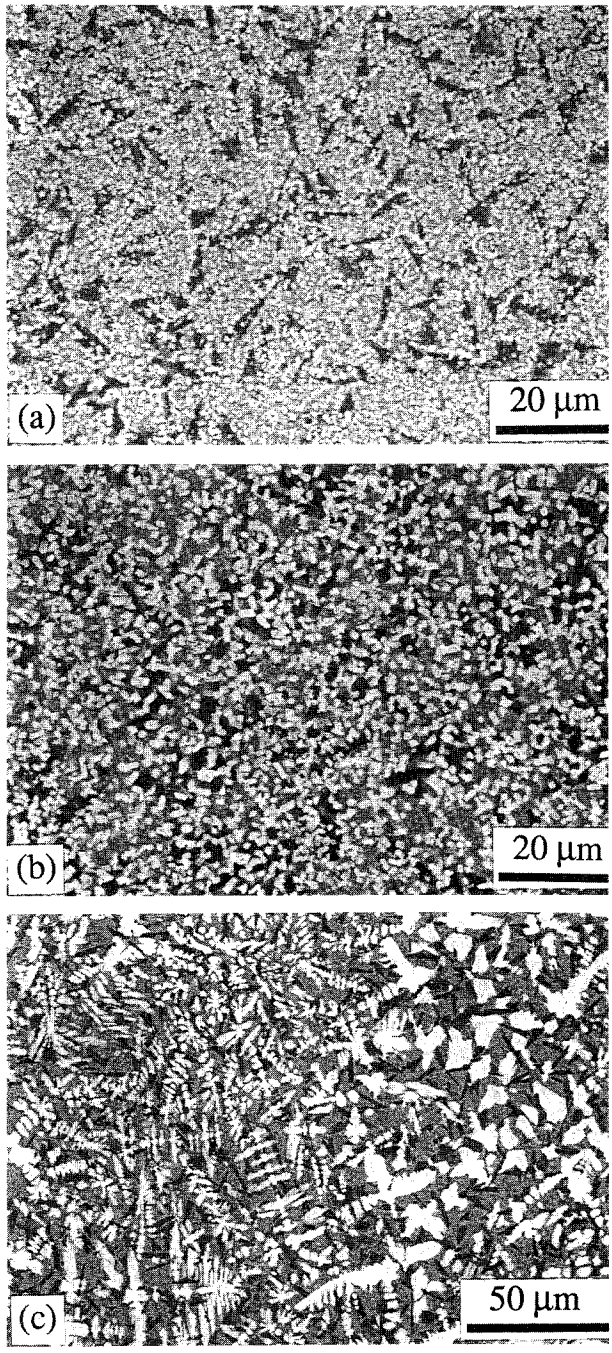

Figure 17 Microstructures of LZS glass-ceramics containing 2 mol % NiO: (a) with no sealing cycle, (b, c) with a sealing cycle.

wide range, depending on the heat-treatment conditions, from ≈ 14.4–16.7×10^{-6} °C (20–550 °C). From the ambient and high-temperature X-ray diffraction data, it was concluded that the overall shape of the thermal expansion curve is due directly to a number of solid state phase transformations occurring as a function of temperature. As illustrated in Fig. 20, the low-temperature transformation is due to an α- to β-cristobalite inversion. The higher temperature behaviour is due to a combination of an α- to β-quartz transformation, and the start of a γ_0- to β_{11}-Li_2ZnSiO_4 transformation. For samples containing β_1-Li_2ZnSiO_4, it may be expected that the corresponding β_1- to β_{11}-Li_2ZnSiO_4 phase transformation will also occur in this temperature regime. The thermal expansion behaviour at temperatures greater than about 500 °C is complicated further due to the presence of a residual glassy phase with a higher T_g than the original LZS glass (the DMTA data indicate that the T_g of this residual glass is of the order of 530 °C). The thermal expansion coefficient goes through a minimum over the crystallization temperature range 825–900 °C. Examination of the X-ray data over this range (Fig. 11e) indicates changes in the presence of the silica polymorphs, with the concentration of cristobalite being lowest at the lower expansion. The thermal expansion behaviour can be modified further by the presence of transition metal oxide additives, and the range can be extended from ≈ 11.5 to 19.3×10^{-6} °C (20–550 °C). Although the α- to

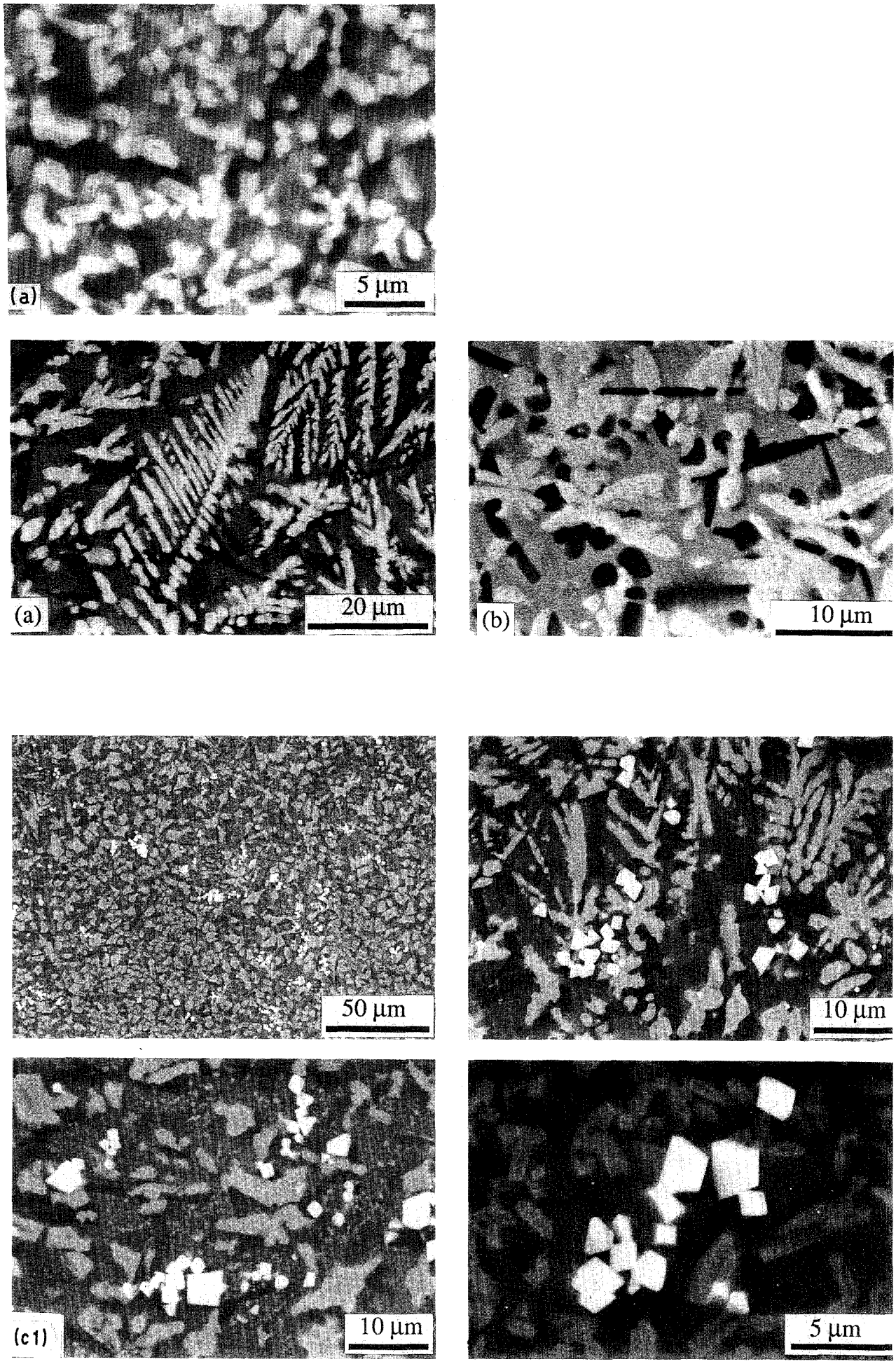

Figure 18 High-magnification micrographs of LZS glass-ceramics containing TMO additions (with a high-temperature sealing stage): (a) TiO_2, (b) Nb_2O_5, (c) Cr_2O_3, (d) WO_3, (e) NiO.

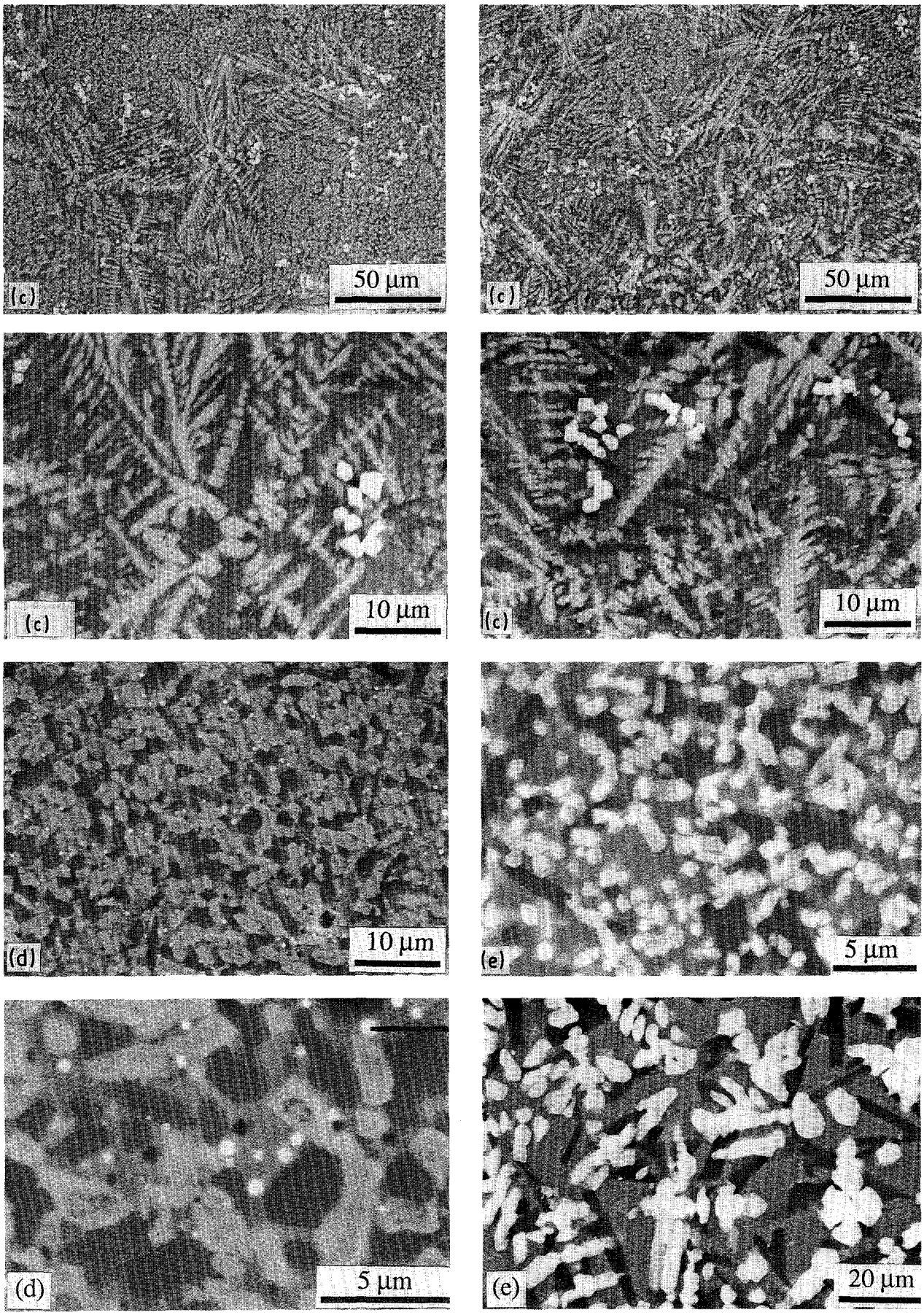

Figure 18 Continued.

β-cristobalite inversion is absent or not as well pronounced for some of the glass-ceramics containing the TMO additions, a number of these materials do, however, exhibit high expansions over the higher temperature range (i.e. 20–550 °C), apparently due to a high concentration of quartz, as noted in the X-ray data for vanadium, for example Fig. 11f. In general, in the absence of a high-temperature simulated sealing

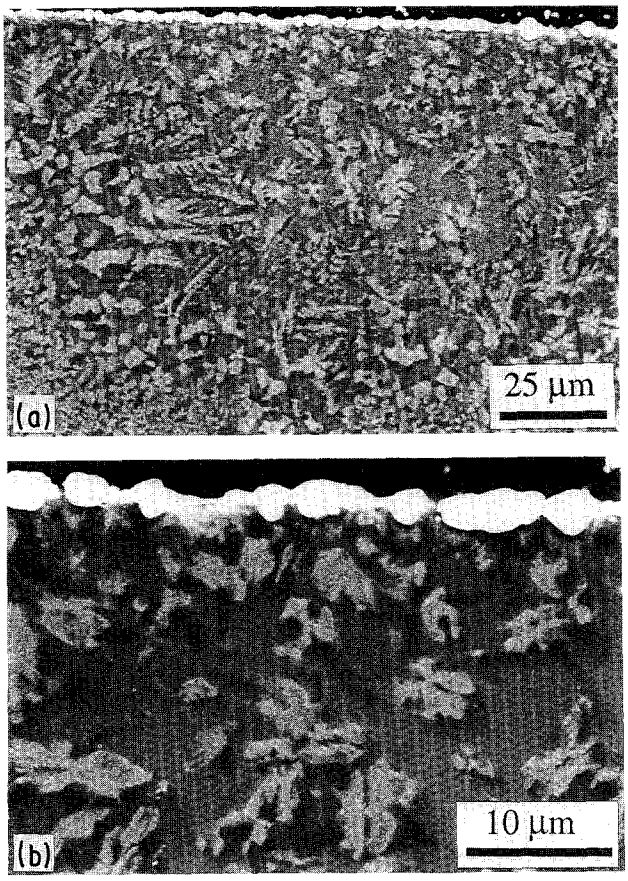

Figure 19 (a, b) Micrographs of LZS glass-ceramic containing CuO. A layer of metallic copper is visible on the surface.

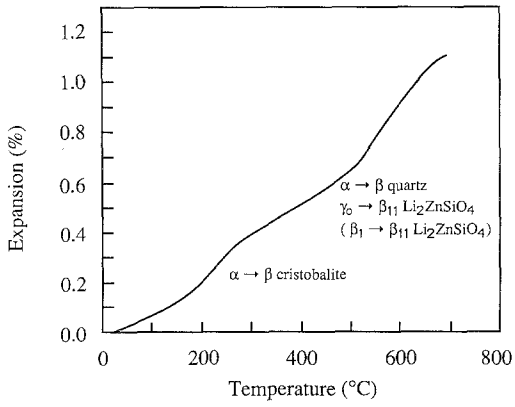

Figure 20 Representative thermal expansion curve for LZS glass-ceramic showing crystal phase changes associated with the characteristic shape of the curve.

stage, the thermal expansion is lowered. For example, for a crystallization temperature of 850 °C a thermal expansion of 14.8×10^{-6} °C (20–550 °C) is observed without a sealing stage, whilst the equivalent value with a sealing stage is 15.6. The range is increased from 14.4 to 16.4 for a crystallization temperature of 800 °C. This overall behaviour makes the LZS system an extremely versatile glass-ceramic for matching of thermal expansion to a wide range of materials.

The microstructures of the resultant glass-ceramics are complex, consisting of several randomly distributed phases. Differences are noted between samples that have been given a high-temperature simulated sealing stage and those that have not, although in general the differences are remarkably small. Of particular note are the following. The glass-ceramic containing Nb_2O_5 consists of relatively large Li_2ZnSiO_4 crystals and a mixture of acicular and equi-axed silica grains is apparent; in many instances the silica appears to have been nucleated from the Li_2ZnSiO_4 phase. Addition of Ta_2O_5 leads to the loss of the acicular silica and the appearance of a sparse dispersion of small crystals rich in tantalum. For the glass-ceramic containing Cr_2O_3 a microstructure consisting of acicular silica and equi-axed Li_2ZnSiO_4, together with a dispersion of $ZnCr_2O_4$ crystals is observed; when a sealing cycle is included, an additional coarse dendritic structure is noted. Samples containing NiO and TiO_2 have also been observed to contain some dendritic structures if a sealing stage is included. Addition of MoO_3 gives rise to a structure consisting of relatively large acicular silica grains (up to ≈ 20 μm in length), but this is coupled with an extremely fine Li_2ZnSiO_4 grain size (≈ 0.3 μm). The sample containing WO_3 contains a dispersion of tungsten-rich spherical particles. Heat treatment of the CuO- and NiO-containing glasses produces a layer of metallic copper or nickel on the surface of the resultant glass-ceramics. A similar effect has been noted for glass-ceramics containing CuO by McMillan and Hodgson [4]. These authors suggested that such materials may be useful for producing printed circuit boards and other similar electronic components.

It is generally agreed (e.g. [24–26, 32–36]) that the use of variable heating rate methods, i.e. the Kissinger [27] or Ozawa [32] techniques, for the determination of kinetic data is directly applicable only to the derivative thermoanalytical curve. This is most closely satisfied for power-compensated differential scanning calorimetry, where the peak of the crystallization exotherm corresponds more closely to the maximum rate of the transformation than is the case when using classical DTA. For DTA, the maximum rate of transformation is generally expected to occur at some point prior to the peak of the curve. Little work has been reported in which kinetic data have been obtained and compared directly for a given glass using DTA, DSC and isothermal methods. Limited work has suggested, however, that DTA methods may give similar results to those obtained using either power-compensated DSC [37], or even isothermal methods [38]. More generally, it has been suggested [24–26] that use of a modified Kissinger equation can be employed to give more meaningful results directly from DTA data, if the precise crystallization mechanism is known. Use is then made of the modified Kissinger equation (Equation 1) by employing the appropriate values of the crystallization parameters, n and m, given in Table III. In the present work well-nucleated samples were employed. Micrographical evidence also indicates that crystallization generally occurs to give three-dimensional grains. (Although acicular grains are also observed, these generally have relatively low aspect ratios.) Values of $n = m = 3$ were therefore considered appropriate. It cannot be stressed strongly enough, of

course, that the activation energies so obtained using variable heating rate methods are *apparent* activation energies, and may be the compound result of a number of simultaneous events, e.g. crystallization of more than one phase. Data so derived can, nevertheless, be very useful in determining overall trends in crystallization behaviour. This is especially true when a qualitative comparison is required between, for example, the nucleating efficiencies of various candidate nucleating species.

From the kinetic data obtained in the present work (Table VI) it is clear that some of the TMO additions have a very pronounced influence on the activation energies for crystallization. On analysis of these data, a broad trend was noted between the activation energy and the ionic field strength of the TM ion species, with activation energy decreasing with increasing field strength, as illustrated in Fig. 21. This indicates that TM ions of high charge and/or relatively small size, in particular vanadium, molybdenum and tungsten, destabilize the LZS glass (strictly speaking the supercooled liquid) and are therefore particularly effective as crystallization aids. As noted by McMillan [39], interstitial cations of high field strength will tend to disturb the silicate network by creating a strong ordering influence due to the strict co-ordination number requirements. This effect may induce or enhance phase separation of the glass or may lead to the formation of small crystallites. That such additives can indeed act as powerful nucleating agents in silicate systems is well established (e.g. [39]), although little systematic work has been reported on the relative nucleating efficiencies of a wide range of additions on a single glass composition. The present study has shown, therefore, for this particular LZS system, that nucleating efficiency as measured by the activation energy for crystallization, is indeed directly related to the relative ionic field strength of the additive employed.

Finally, as has been noted previously by the present authors [15], the simple nucleating efficiency test, in which the difference in crystallization temperatures between coarse and fine samples of glass is employed as a measure of the nucleation efficiency, cannot be used to give reliable data, unless samples are pre-nucleated. For example, as-quenched samples of LZS glass with and without addition of the oxides of niobium and tungsten give large deviations between the crystallization temperatures of coarse and fine samples; if these samples are pre-nucleated, however, these differences are reduced (Table V).

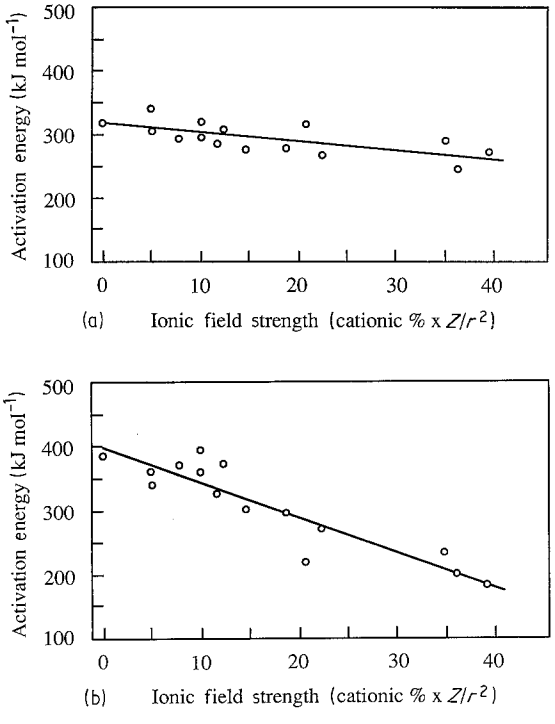

Figure 21 Activation energy for crystallization as a function of the ionic field strength of the TM solute ion species. (a) First crystallization exotherm, (b) second crystallization exotherm.

5. Conclusions

1. Two crystallization exotherms are resolved in DTA scans of the lithium zinc silicate composition described in the present work, with apparent activation energies of 319 and 389 kJ mol^{-1}, respectively. Addition of transition metal oxides to the LZS glass alters the crystallization kinetics markedly. In particular, addition of 3.5 mol % MoO_3 reduces the activation energies to 219 and 203 kJ mol^{-1}, respectively; and 3.5 mol % WO_3 reduces them to 274 and 183 kJ mol^{-1} respectively.

2. The apparent activation energy for crystallization is broadly related to the ionic field strength of the TM ion solute species, crystallization being favoured by TM solutes of high field strength, i.e. high charge and/or small size.

3. The optimum nucleation temperature for the LZS glass, determined by a DTA method, is 465 °C. Data from DMTA and SANS suggest that the nucleated glass is phase separated, the SANS data indicating that this is on a very fine scale, of the order of 16 nm.

4. The ternary LZS glass-ceramic has been found to consist of α-cristobalite, α-quartz and γ_0-Li_2ZnSiO_4 crystalline phases. The equivalent LZS composition which contains the extra oxide additions, i.e. Na_2O, B_2O_3 and P_2O_5, is more complex. Depending on the precise heat-treatment conditions, some of these glass-ceramics have been found to contain varying proportions of cristobalite, quartz and tridymite, together with γ_0- and β_1-Li_2ZnSiO_4. In many instances, the LZS phase cannot be identified positively, possibly because of lattice distortion associated with incorporation of some of the extra constituents into the structure.

5. The microstructures of the LZS glass-ceramics are complex, consisting of a number of different grain morphologies including small (≈ 1 μm) equi-axed grains, larger acicular grains and residual glass. The transition metal oxide additions have a pronounced effect on the resultant microstructures. In particular, MoO_3 reduces the size of the equi-axed grains (to ≈ 0.3 μm), whilst Cr_2O_3 yields a dispersion of zinc chromate crystals, and WO_3 gives a dispersion of spherical tungsten-rich particles. The microstructures

of samples that have been subjected to an additional high-temperature simulated sealing stage are in general remarkably similar, although some samples exhibit additional dendritic structures.

6. The LZS composition can be used to prepare moderately high thermal expansion glass-ceramics, with α in the range $14.4–16.7 \times 10^{-6}\,°C^{-1}$ (20–550 °C), the precise expansion depending on the heat-treatment conditions employed. Variations in the thermal expansion behaviour can be ascribed to varying concentrations and ratios of the silica polymorphs cristobalite, quartz and tridymite.

7. Addition of 2 mol % transition metal oxides to the LZS glass modifies the thermal expansion behaviour of the resultant glass-ceramics. Depending on the specific additive employed, expansions in the range $11.5–18.4 \times 10^{-6}\,°C^{-1}$ (20–550 °C) can be achieved. Variations in the thermal expansion behaviour can again be ascribed to varying concentrations and ratios of the silica polymorphs cristobalite, quartz and tridymite.

Acknowledgements

We thank Mrs E. A. Prior and Mr C. Ruckman, AWE, for carrying out the optical and electron microscopy, and Messrs M. Clay and T. Carter, AWE, for the ambient temperature X-ray diffraction studies. We are also very grateful to Dr R. Hill and Mr P. Gilbert, Thames Polytechnic, for carrying out the DMTA analyses. In addition we thank Dr S. Tarling, Birkbeck College, for the high temperature X-ray diffraction data, Dr R. K. Heenan, Rutherford Laboratory, for the small-angle neutron scattering results, Dr S. Carter, Imperial College, for carrying out the transmission electron microscoy, and Pilkington Technology Centre for the viscosity measurements. This paper is published with permission of the Controller, HMSO, holder of Crown Copyright.

References

1. P. W. McMILLAN and G. PARTRIDGE, Brit. Pat. 943 599 (1963).
2. P. W. McMILLAN, B. P. HODGSON and G. PARTRIDGE, *Glass Technol.* **7** (1966) 121.
3. P. W. McMILLAN, G. PARTRIDGE, B. P. HODGSON and H. R. HEAP, *ibid.* **7** (1966) 128.
4. P. W. McMILLAN and B. P. HODGSON, Brit. Pat. 944 571 (1963).
5. P. W. McMILLAN and G. PARTRIDGE, *Proc. Brit. Ceram. Soc.* **3** (1965) 241.
6. P. W. McMILLAN, B. P. HODGSON and G. PARTRIDGE, US Pat. 3220 815 (1965).
7. P. W. McMILLAN and G. PARTRIDGE, US Pat. 3170 805 (1965).
8. P. W. McMILLAN and B. P. HODGSON, Brit. Pat. 1023 480 (1966).
9. *Idem.*, Brit. Pat. 1063 291 (1967).
10. B. L. METCALFE and I. W. DONALD, "Effect of composition on the sealing behaviour of lithium zinc silicate glass-ceramics", paper presented at the Symposium on Glass in Electronics, Society of Glass Technology, Blackpool, 11–12 May, 1989.
11. *Idem.*, in "The International Conference on New Materials and their Applications", University of Warwick, April 1990, Institute of Physics Conference Series no. 111, edited by D. Holland (IOP, Bristol, 1990) pp. 469–78.
12. B. L. METCALFE, I. W. DONALD and D. J. BRADLEY, in "Proceedings of the Conference on Surfaces and Interfaces", Interceramex, NEC, Birmingham, October 1990, Institute of Ceramics Proceedings No. 48, edited by R. Morrell and G. Partridge (ICS, Stoke, 1991) pp. 177–188.
13. A. R. WEST and F. P. GLASSER, *J. Mater. Sci.* **5** (1970) 557.
14. *Idem., ibid.* **5** (1970) 676.
15. I. W. DONALD, B. L. METCALFE, D. J. WOOD and J. R. COPLEY, *ibid.* **24** (1989) 3892.
16. Z.-X. CHEN and P. W. McMILLAN, *J. Amer. Ceram. Soc.* **68** (1985) 220.
17. S.-B. LEE and S-M. HAN, *J. Korean Ceram. Soc.* **24** (1987) 227, in Korean.
18. B. B. RAO, N. K. REDDY and M. A. JALEEL, *J. Mater. Sci. Lett.* **9** (1990) 1159.
19. R. L. THAKUR and S. THIAGARAJAN, *Glass Ceram. Bull.* **13** (1966) 33.
20. A. MAROTTA, A. BURI and F. BRANDA, *J. Mater. Sci.* **16** (1981) 341.
21. A. MAROTTA, S. SAIELLO, F. BRANDA and A. BURI, *Verres Réfract* **35** (1981) 477.
22. S. SAIELLO, F. BRANDA, A. BURI and A. MAROTTA, *ibid.* **36** (1982) 859.
23. A. MAROTTA, A. BURI, F. BRANDA and S. SAIELLO, in "Advances in Ceramics 4", edited by J. H. Simmons, D. R. Uhlmann and G. H. Beall (American Ceramic Society, Columbus, 1982) pp. 146–52.
24. K. MATUSITA, S. SAKKA and Y. MATSUI, *J. Mater. Sci.* **10** (1975) 961.
25. K. MATUSITA and S. SAKKA, *J. Non-Cryst. Solids* **38,39** (1980) 741.
26. *Idem., Bull. Inst. Chem. Res. Kyoto Univ.* **59** (1981) 159.
27. H. E. KISSINGER, *J. Res. Nat. Bur. Stand.* **57** (1956) 217.
28. P. K. GILBERT, MSc thesis, Thames Polytechnic (1989).
29. R. G. HILL and P. K. GILBERT, *J. Amer. Ceram. Soc.* in press.
30. P. C. JENNINGS, B. L. METCALFE and I. W. DONALD, AWE (1990) unpublished work.
31. I. M. STEWART and G. J. P. BUCHI, *Trans. Brit. Ceram. Soc.* **61** (1962) 615.
32. T. OZAWA, *J. Thermal Anal.* **9** (1976) 369.
33. R. L. REED, L. WEBER and B. S. GOTTFRIED, *IEC Fund.* **4** (1965) 38.
34. J. H. SHARP, in "Differential Thermal Analysis", edited by R. C. Mackenzie (Academic Press, London, 1972) pp. 47–77.
35. E. BAIOCCHI, M. BETTINELLI, A. MONTENERO, L. DI SIPIO and A. SOTGIU, *J. Mater. Sci.* **18** (1983) 411.
36. J. SESTAK, *J. Thermal Anal.* **30** (1985) 1223.
37. W. F. HAMMETTER and R. E. LOEHMAN, *J. Amer. Ceram. Soc.* **70** (1987) 577.
38. H. G. WANG, H. HERMAN and X. LUI, *J. Mater. Sci.* **25** (1990) 2339.
39. P. W. McMILLAN, "Glass Ceramics", 2nd Edn (Academic Press, London, 1979).

Received 6 February
and accepted 14 June 1991